Submitted to Proceedings of
Int. Conf. on π-π Scattering
and Associated Topics,
Florida State Univ, March 28-30, 1973

April 1973

BNL 17846

AMPLITUDE ANALYSES OF HYPERCHARGE EXCHANGE REACTIONS*†

Conf-730319--4

R. D. Field
Brookhaven National Laboratory, Upton, New York 11973

ABSTRACT

The determination of the two-body production amplitudes for Y=1 exchange reactions is discussed. The pseudoscalar production line reversed reactions $K^-n \to \pi^-\Lambda$ and $\pi^-p \to K^0\Lambda$; the vector-meson production reactions $K^-p \to (\omega,\varphi)\Lambda$ and $\pi^-p \to K^{*0}\Lambda$; the reaction $K^-p \to \pi^-Y^{*+}(1385)$; and the photoproduction reaction $\gamma p \to K^+\Lambda$ are examined. Quark model, SU(3), and VDM comparisons are made and the EXD nature of the K^{**} and K^* Regge exchanges explored. In addition the behavior of the unnatural parity Y=1 exchanges (K, K_B, K_A) are investigated

I. INTRODUCTION

It has become increasingly evident throughout this conference that before substantial new progress can be made on the determination of π-π and K-π scattering one must have a better knowledge of the behavior of two-body production amplitudes. This is crucial in order to decide upon proper extrapolation procedures. Due to the self-analysing property of the Λ (and Σ) hyperon reactions with Y=1 exchange provide much information on the nature of production processes. Although the decay correlations from unpolarized initial particles are insufficient for a complete determination of the productions amplitudes, observing all the decay products affords one the opportunity of determining a nearly complete set.[1] By judiciously choosing the set of independent amplitudes (transversity type) the unknown quantities are one relative phase φ_R and one overall phase φ_0. In spite of the lack of knowledge of these two phases, one can learn a great deal about the behavior of these amplitudes.

In Sec. II the reactions $K^-n \to \pi^-\Lambda$ and $\pi^-p \to K^0\Lambda$ are discussed and a comparison of various models is presented. By observing the two-step decay of the Y*(1385) one can determine much about the amplitudes for the reaction $K^-p \to \pi^-Y^{*+}(1385)$. This is discussed and experimental results shown in Sec. III. In Sec. IV vector-meson production with Y=1 exchange is examined. New results for the amplitudes in $K^-p \to (\omega,\varphi)\Lambda$ are presented and compared with previous analyses for $\pi^-p \to K^{*0}\Lambda$. The similarities between the vector meson production reactions $K^-p \to (\omega,\varphi)\Lambda$ and the pseudoscalar production reactions $K^-n \to \pi^-\Lambda$ and $\pi^-p \to K^0\Lambda$ are discussed. In Sec. V SU(3)

*Invited talk presented at the International Conference on π-π Scattering and Associated Topics held at Florida State University, March 28-30, 1973.

†Work performed under the auspices of the U. S. Atomic Energy Commission.

and VDM are used to predict observables for the photoproduction reaction $\gamma p \to K^+\Lambda$ from the amplitudes for $K^-p \to (\omega,\varphi)\Lambda$. In Sec. VI we present a summary and discuss interesting future experimental observations. The definitions of transversity amplitudes and many useful relations including the connection between the transversity amplitudes and the s- and t-channel helicity amplitudes are presented in the Appendix.

II. PSEUDOSCALAR PRODUCTION WITH Y = 1 EXCHANGE ($K^-n \to \pi^-\Lambda$, $\pi^-p \to K^0\Lambda$)

The two body production process $PB \to P'B'$ can be described at each value of s and t by four complex transversity amplitudes $T_{\lambda'\lambda}(s,t)$, where $\lambda'(\lambda)$ corresponds to the component of spin of the outgoing baryon B' (target baryon B) along the transversity z-axis defined normal to the production plane (see Appendix). The two amplitudes T_{+-} and T_{-+} vanish by parity (A.3) leaving the two independent complex amplitudes $T_{++}(s,t)$, $T_{--}(s,t)$ (4 parameters at each s and t). These two transversity amplitudes are related to the helicity amplitudes as follows:

$$H_{++}(s,t) = T_{++}(s,t) + i\,T_{--}(s,t) \tag{2.1a}$$

$$H_{+-}(s,t) = T_{++}(s,t) - i\,T_{--}(s,t) \tag{2.1b}$$

and the helicity amplitudes are related to the observables $\frac{d\sigma}{dt}$ and P by

$$\frac{d\sigma}{dt} \propto |H_{++}|^2 + |H_{+-}|^2 \tag{2.2a}$$

$$P = \frac{2\,\mathrm{Im} H_{++} H_{+-}^*}{|H_{++}|^2 + |H_{+-}|^2} \tag{2.2b}$$

The observables are thus related to the transversity amplitudes by

$$\frac{d\sigma}{dt} \propto |T_{++}|^2 + |T_{--}|^2 \tag{2.3a}$$

$$P = \frac{|T_{++}|^2 - |T_{--}|^2}{|T_{++}|^2 + |T_{--}|^2} \tag{2.3b}$$

Thus by observing the Λ polarization (Λ decay) in addition to the differential cross section one can determine the magnitudes of the two transversity amplitudes for the reactions $K^-n \to \pi^-\Lambda$ and $\pi^-p \to K^0\Lambda$. One cannot determine the relative phase between the two amplitudes φ_R ($\varphi_R = \mathrm{Arg}(T_{++}) - \mathrm{Arg}(T_{--})$) nor can one determine the overall phase of the amplitudes φ_0. At each value of s and t one can determine two of the four parameters necessary to completely describe the reactions. The relative phase φ_R can only be determined by including polarized target information (A and R parameters).

From (2.1a,b) it is seen that without a knowledge of the relative phase φ_R the structures of the helicity amplitudes H_{++} and H_{+-} are unknown (both the magnitudes and phases of the helicity amplitudes

depend on φ_R). Nevertheless the determination of $d\sigma/dt$ and P (i.e. $|T_{++}|^2$ and $|T_{--}|^2$) for the line reversed reactions $K^-n \to \pi^-\Lambda$ and $\pi^-p \to K^0\Lambda$ tells us much about the production process. (Strictly speaking $\pi^+n \to K^+\Lambda$ is the line reversed partner of the reaction $K^-n \to \pi^-\Lambda$ but $A(\pi^+n \to K^+\Lambda) = A(\pi^-p \to K^0\Lambda)$ by isospin.)
The important features of the experimental data on $K^-n \to \pi^-\Lambda$ and $\pi^-p \to K^0\Lambda$ are:

(1) The differential cross sections for the two reactions are not equal. (Fig. 1) The differential cross section for $\pi^-p \to K^0\Lambda$ is steeper and smaller at large $|t|$. The two cross sections do appear to agree in the forward direction.

(2) The polarization for the two reactions are both non-zero and they have the same sign for $0 \lesssim |t| \lesssim 0.4$ $(GeV/c)^2$ (Fig. 2). Figure 2 also shows the magnitudes of the transversity amplitudes, where we have normalized so that $|T_{++}|^2 + |T_{--}|^2 = 1$.

The above experimental observations place great restrictions on high energy models attempting to describe reactions $K^-n \to \pi^-\Lambda$ and $\pi^-p \to K^0\Lambda$ which only have natural parity exchange (K^{**},K^*) in the t-channel. The high energy models for these reactions can be divided into three types. First, there are models that attempt to describe these reactions in terms of Regge poles (K^{**},K^*) only with no absorption:

Type 1a: Duality and EXD pole model - The duality diagram for $K^-n \to \pi^-\Lambda$ is non-planar (quark lines cross), whereas the diagram for $\pi^-p \to K^0\Lambda$ is planar (no crossed quark lines). Thus, the s-channel helicity amplitudes for $K^-n \to \pi^-\Lambda$ are predicted to be purely real and those for $\pi^-p \to K^0\Lambda$ are predicted to have a rotating phase $\exp(-i\pi\alpha(t))$.[2] These predictions are identical to the ones arrived at by assuming that the K^{**} and K^* Regge poles are strongly EXD. The model predicts

$$\frac{d\sigma}{dt}(K^-n \to \pi^-\Lambda) = \frac{d\sigma}{dt}(\pi^-p \to K^0\Lambda) \qquad (2.4a)$$

and

$$P(K^-n \to \pi^-\Lambda) = P(\pi^-p \to K^0\Lambda) = 0 \qquad (2.4b)$$

in obvious disagreement with the data.

Type 1b: Weakly EXD pole models - This model assumes only the trajectory functions of the K^{**} and K^* pole are equal and not the residues. This model predicts

$$\frac{d\sigma}{dt}(K^-n \to \pi^-\Lambda) = \frac{d\sigma}{dt}(\pi^-p \to K^0\Lambda) \qquad (2.5a)$$

and

$$P(K^-n \to \pi^-\Lambda) = -P(\pi^-p \to K^0\Lambda) \quad , \qquad (2.5b)$$

which disagrees with experiment.

Type 1c: Broken EXD pole model - In this model EXD is broken in both the residue and trajectory functions for the K^{**} and K^* pole. This model predicts

$$P\,\frac{d\sigma}{dt}(K^-n \to \pi^-\Lambda) = -P\,\frac{d\sigma}{dt}(\pi^-p \to K^0\Lambda) \quad . \tag{2.6}$$

This prediction is also in disagreement with the data since the polarization for $K^-n \to \pi^-\Lambda$ and $\pi^-p \to K^0\Lambda$ have the same sign for small $|t|$ (see Fig. 2). The K** and K* Regge poles are thus inadequate to describe these reactions no matter how much EXD is broken![3-4] One must introduce absorptive corrections and/or lower lying poles.

The second class of models are those that assume the bare K** and K* poles are EXD, and add absorptive corrections and/or lower lying poles in an attempt to explain the experimental data.

Type 2a: EXD poles plus "old" absorption[5]- This model assumes that the bare K** and K* Regge poles are EXD and that the EXD is broken by introducing absorptive corrections. The absorptive corrections (Regge cuts) are calculated using the "old" absorption model which calculates the partial wave projection of the cut H^J_{cut} using the Sopkovich prescription[6]

$$H_{cut}{}^J(s) = iH^J_{pole}(s)H^J_{elastic}(s) \tag{2.7}$$

where $H^J_{pole}(s)$ is the partial wave projection of the s-channel Regge pole helicity amplitude and $H^J_{elastic}(s)$ is the s-channel helicity partial wave projection of the elastic amplitude given by a Pomeron amplitude of the form

$$H_{Pomeron}(s,t) = is\sigma_{tot}\left(\frac{s}{s_0}\,e^{\frac{-i\pi}{2}}\right)^{\alpha' t}\; e^{\frac{A}{2}t} \quad . \tag{2.8}$$

This type of model is able to explain the behavior of the polarizations in $K^-n \to \pi^-\Lambda$ and $\pi^-p \to K^0\Lambda$ but predicts

$$\frac{d\sigma}{dt}(\pi^-p \to K^0\Lambda) \;>\; \frac{d\sigma}{dt}(K^-n \to \pi^-\Lambda) \tag{2.9}$$

in disagreement with the data.

Type 2b: EXD poles plus "old" absorption plus daughters[7]- This model is identical to type 2a but with the addition of daughter trajectories. The daughter trajectories do not affect the model's ability to successfully fit the polarizations, but allows one to also fit the differential cross sections. Since the line reversal breaking of the differential cross sections is attributed to lower lying daughter trajectories, this model predicts

$$\frac{d\sigma}{dt}(K^-n \to \pi^-\Lambda) \to \frac{d\sigma}{dt}(\pi^-p \to K^0\Lambda)$$

as energy is increased.

Due to the inability of the "old" absorption model to successfully explain line reversal breaking, "new" absorption models were invented. The next class of models abandon the prescription of (2.7) and (2.8) in favor of a phenomenological prescription for calculating Regge cuts.

Type 2c: EXD poles plus phenomenological absorption[8-10]These models are constructed to absorb real and imaginary parts differently. One finds that to explain the data one must absorb the imaginary parts more than the real parts. Thus, for example, the real reaction ("1") $K^-n \to \pi^-\Lambda$ is absorbed less than the rotating reaction ($e^{-i\pi\alpha(t)}$)

$\pi^- p \to K^0\Lambda$ providing

$$\frac{d\sigma}{dt}(K^- n \to \pi^-\Lambda) > \frac{d\sigma}{dt}(\pi^- p \to K^0\Lambda)$$

in accordance with the data.

Type 2d: T_{eff} absorption models[11,12] - Strictly speaking this type should not be called a model. For this method one calculates the absorption according to

$$H^J_{cut}(s) = i\, H^J_{pole}\, T^J_{eff} \qquad (2.10)$$

and determines what kind of T^J_{eff} is necessary to fit the data. Different T^J_{eff}'s arise depending on the assumptions concerning the initial Regge poles. Barger and Martin[13] assume EXD K** and K* poles and no absorption in the s-channel flip amplitude. They then determine the structure of the non-flip amplitudes (pole + cut) necessary to fit the data. The results are interesting but depend, of course, on their initial assumptions.

The next type of model abandons the assumption of EXD bare Regge poles.

Type 3a: Non-EXD pole (no WSNZ) plus "old" absorption.[14] This is just the old SCRAM model. It assumes no wrong signature zero (WSNZ) of the Regge pole and produces dips by pole-cut interference. This model can fit the observables for $K^- n \to \pi^-\Lambda$ and $\pi^- p \to K^0\Lambda$. The ability to fit the behavior of the differential cross sections is due to the relaxing of the EXD of the bare poles. There are, however, other reactions where this model fails badly (e.g., $\pi^- p \to \pi^0 n$).[15]

Type 3b: Non-EXD pole (no WSNZ) plus "fancy" Pomeron absorption - This model, recently proposed by G.L. Kane,[16] assumes broken EXD for the bare poles (no WSNZ). Absorption effects are calculated using (2.10) with $T_{eff} = P+D$, where P corresponds to the Pomeron parametrized by

$$P(s,t) = is\left[Ae^{Bt} + A_0 e^{B_0 t}\, J_0\left(R_0\sqrt{-t}\sqrt{\ell n s - i\,\tfrac{\pi}{2}}\right)\right].$$

The quantity D represents an attempt to include the contributions from the sum over intermediate states other than the elastic one, and is parameterized by

$$D_n(s,t) = is\, e^{Dt}\, J_n\left(R_0\sqrt{-t}\sqrt{\ell n s - i\,\tfrac{\pi}{2}}\right),$$

where n is the net helicity flip. One feature of this T_{eff} is that it has a larger real part than previous models. Hartly and Kane[16] have successfully fit the systematics of many reactions using this model including the reactions $K^- n \to \pi^-\Lambda$ and $\pi^- p \to K^0\Lambda$.[17]

In order to determine which of the above models is a correct description of two-body production, if any, or to decide which features of these models should be retained in future models, it will be necessary to know:

(1) The energy dependences of $d\sigma/dt$ and P for the line reversed reactions $K^- n \to \pi^-\Lambda$ and $\pi^- p \to K^0\Lambda$.

(2) The relative phase φ_R which can be determined by polarized target experiments (with a component of polarization in the production plane).

Table I summarizes the various models applied to the reactions $K^- n \to \pi^-\Lambda$ and $\pi^- p \to K^0\Lambda$.

III. THE REACTION $K^-p \to \pi^- Y^{*+}(1385)$

The reaction $K^-p \to \pi^- Y^{*+}(1385)$ is described by the transversity amplitudes $T_{2\lambda;2\lambda'}(s,t)$, where λ (λ') corresponds to the component of spin of the Y^* (target proton) along the transversity z-axis, which is normal to the production plane (see Appendix). Parity conservation (A.3) implies $T_{31} = T_{1\,-1} = T_{-1\,1} = T_{-3\,-1} = 0$. The remaining four complex amplitudes are related to the eight traneversity density matrix elements as follows:

$$\rho_{33} = |T_{3\,-1}|^2 \tag{3.1a}$$

$$\rho_{11} = |T_{11}|^2 \tag{3.1b}$$

$$\rho_{-1\,-1} = |T_{-1\,-1}|^2 \tag{3.1c}$$

$$\rho_{-3\,-3} = |T_{-31}|^2 \tag{3.1d}$$

$$\mathrm{Re}\rho_{3\,-1} = \mathrm{Re}(T_{3\,-1}T^*_{-1\,-1}) = |T_{3\,-1}||T_{-1\,-1}|\cos\delta_1 \tag{3.1e}$$

$$\mathrm{Im}\rho_{3\,-1} = \mathrm{Im}(T_{3\,-1}T^*_{-1\,-1}) = |T_{3\,-1}||T_{-1\,-1}|\sin\delta_1 \tag{3.1f}$$

$$\mathrm{Re}\rho_{1\,-3} = \mathrm{Re}(T_{11}T^*_{-31}) = |T_{11}||T_{-31}|\cos\delta_2 \tag{3.1g}$$

$$\mathrm{Im}\rho_{1\,-3} = \mathrm{Im}(T_{11}T^*_{-31}) = |T_{11}||T_{-31}|\sin\delta_2 \ , \tag{3.1h}$$

where (A.5b) was used and where δ_1 [δ_2] is defined as the relative phase between the amplitudes $T_{3\,-1}$ and $T_{-1\,-1}$ [T_{11} and T_{-31}].

By observing the two step decay of the $Y^*(1385)$ (i.e., $Y^* \to \pi\Lambda$, $\Lambda \to \pi p$) in addition to the differential cross section for $K^-p \to \pi^- Y^{*+}$ one can determine all the transversity density matrix elements and thus the magnitudes of all four transversity amplitudes and the two relative phases δ_1 and δ_2. Without a polarized target one cannot determine the relative phase φ_R between the amplitudes with target proton transversity up ($\lambda' = 1/2$) and the amplitudes with target proton transversity down ($\lambda' = -1/2$). In addition one, of course, cannot determine the overall phase of the amplitudes φ_0. One can thus determine 6 out of the 8 parameters needed at each s and t value to completely specify the production process $K^-p \to \pi^- Y^{*+}$. The transversity density matrix elements and the phases δ_1 and δ_2 resulting from an analysis of $K^-p \to \pi^- Y^{*+}(1385)$[18] are displayed in Fig. 3, where the density matrix elements are normalized according to

$$\rho_{33} + \rho_{11} + \rho_{-1\,-1} + \rho_{-3\,-3} = 1 \ .$$

The simple non-relativistic additive quark model assumes that the transversity amplitudes for production process $K^-p \to \pi^- Y^*$ can be represented by a sum of quark-quark scattering amplitudes (Fig. 4a).[19] Transversity amplitudes that require a flip of more than one of the baryon quarks, such as $T_{3\,-1}$ (Fig. 4b), are not allowed and predicted to be zero. This model thus predicts

$$T_{3\,-1}(s,t) = T_{-31}(s,t) = 0 \ . \tag{3.2a}$$

It also predicts

$$T_{11}(s,t) = T_{-1\,-1}(s,t) \quad , \tag{3.2b}$$

since these amplitudes are given by the same sum over quark-quark amplitudes. The model thus predicts that $\rho_{11} = \rho_{1-1} = 1/2$ and that the remaining transversity density matrix elements vanish. As can be seen from the data in Fig. 3 these predictions do explain the gross features of the amplitudes, however, they are not satisfied exactly. The data clearly show non-zero values of ρ_{33}, $\mathrm{Im}\rho_{3\,-1}$, and $\mathrm{Re}\rho_{3\,-1}$ in the small momentum transfer region $|t_0-t| \lesssim 0.3$ (GeV/c)^2 indicating a non vanishing $T_{3\,-1}$ amplitude.

By the use of (A.4) the quark model predictions for the transversity amplitudes can be converted into a prediction about the s-channel helicity amplitudes. Namely,

$$H_{3/2;-1/2}(s,t) = H_{1/2;1/2}(s,t) = 0$$

and

$$H_{3/2;1/2}(s,t) = \sqrt{3}\ H_{1/2;-1/2}(s,t)$$

which implies (using (A.5a)) that $\rho^H_{33} = 3/8$, $\mathrm{Re}\rho^H_{3\,-1} = \sqrt{3}/8$ and that the remaining s-channel density matrix elements vanish. These are the same as the Stodolsky-Sakurai predictions for ρ exchange in the reaction $\pi N \to \pi\Delta(1236)$. The s-channel density matrix elements for $K^-p \to \pi^- Y^{*+}$ are shown in Fig. 5. Again we see rough agreement with the quark model prediction.

IV. VECTOR MESON PRODUCTION WITH Y = 1 EXCHANGE

The twelve complex transversity amplitudes for the reaction $PB \to VB'$, where P and V are pseudoscalar and vector mesons, respectively, and B and B' are spin 1/2+ baryons are written as follows:

$$T^{\mu}_{\lambda'\lambda}(s,t) \quad ,$$

where λ, λ', and μ correspond to the components of spin of the target baryon B, baryon B', and vector meson V, respectively, along the transversity z-axis (see Appendix). Parity conservation implies $T^{\mu}_{\lambda'\lambda}(s,t)$ vanish when $(-1)^{\lambda'-\lambda+\mu}$ is odd. Thus six independent complex amplitudes are sufficient to describe the reaction $PB \to VB'$. These six transversity amplitudes are related to the helicity type amplitudes as follows:

$$\begin{aligned}
T_{++}{}^{0} &= -i\sqrt{2}\ A^{+} & T_{--}{}^{0} &= -i\sqrt{2}\ A^{-} \\
T_{-+}{}^{1} &= iB^{+}+C^{+} & T_{+-}{}^{1} &= iB^{-}+C^{-} \\
T_{-+}{}^{-1} &= -iB^{+}+C^{+} & T_{+-}{}^{-1} &= -iB^{-}+C^{-} \quad ,
\end{aligned} \tag{4.1}$$

where

$$A^{\pm} = \frac{1}{2}\{H^{1}_{++} + H^{-1}_{++} \mp i(H^{1}_{-+} + H^{-1}_{-+})\}$$
$$B^{\pm} = \mp\frac{1}{2}\{H^{1}_{++} - H^{-1}_{++} \pm i(H^{1}_{-+} - H^{-1}_{-+})\}$$
$$C^{\pm} = \mp\frac{1}{\sqrt{2}}(H^{0}_{++} \pm iH^{0}_{-+}) \quad , \qquad (4.2)$$

and where the T's are helicity-transversity amplitudes (Jackson-transversity) when the corresponding H's are s-channel helicity (t-channel helicity) amplitudes. The $A^{\pm}$, $B^{\pm}$ and $C^{\pm}$ amplitudes are simply related to the amplitudes defined by Byers and Yang;[20] the superscripts $\pm$ refer to states with target baryon transversity $\lambda = \pm 1/2$.

Due to the self-analysing property of the Λ hyperon, the reactions $K^-p \to (\omega,\varphi)\Lambda$ and $\pi^-p \to K^{*0}\Lambda$ provide one the opportunity of learning much about the production amplitudes. Indeed observation of the joint density matrix elements between the vector meson V and Λ hyperon, in addition to the single density matrix elements of the vector meson, and the Λ polarization allows determination of the magnitudes of all six transversity amplitudes plus the determination of the relative phases between amplitudes with the same target baryon transversity (λ). The amplitudes can be divided into two sets of three amplitudes

$$\begin{pmatrix} T^{0}_{++} \\ T^{1}_{-+} \\ T^{-1}_{-+} \end{pmatrix} \qquad \begin{pmatrix} T^{0}_{--} \\ T^{1}_{+-} \\ T^{-1}_{+-} \end{pmatrix}$$

for the transversity amplitudes and

$$\begin{pmatrix} A^{+} \\ B^{+} \\ C^{+} \end{pmatrix}, \qquad \begin{pmatrix} A^{-} \\ B^{-} \\ C^{-} \end{pmatrix}$$

for the Byers and Yang type amplitudes. From the joint decay angular distributions of the vector meson V and Λ hyperon together with the differential cross section the amplitudes can be determined up to a relative phase φ_R between the target baryon transversity up ($\lambda = 1/2$) and down ($\lambda = -1/2$) groups and an overall phase φ_0. Thus out of the 12 parameters at each s and t necessary to completly specify the amplitudes, 10 can be determined.

The magnitudes of the transversity amplitudes for $K^-p \to (\omega,\varphi)\Lambda$ are shown in Fig. 6 as a function of momentum transfer, and where we have normalized

$$\sum_{\mu,\lambda',\lambda} |T^{\mu}_{\lambda'\lambda}|^2 = 1 \quad .$$

Figure 7 shows the relative phases

$$\theta^{\pm 1}_{\pm} = \mathrm{Arg}(T^{\pm 1}_{\mp +}) - \mathrm{Arg}(T^{0}_{\pm \pm})$$

for $K^- p \to (\omega,\varphi)\Lambda$ as a function of momentum transfer. As can be seen from Figs. 6 and 7 there are striking differences in the amplitude structure for $K^- p \to (\omega,\varphi)\Lambda$. In particular $K^- p \to \varphi\Lambda$ has large values of $|T^0_{--}|^2$ and small values of $|T^0_{+-}|^2$ while $K^- p \to \omega\Lambda$ has large values of the latter and small values of the former.

Arguments similar to those in Sec. III using the simple quark model lead to the prediction that[19]

$$T^{\mu}_{\lambda',\lambda}(K^- p \to \varphi\Lambda) = T^{\mu}_{\lambda',\lambda}(\pi^- p \to K^{*0}\Lambda) \quad ,$$

which also implies via (4.1) that the $A^{\pm}_{\mp}$, $B^{\pm}_{\mp}$, $C^{\pm}_{\mp}$ amplitudes are identical. Figure 8 shows a comparison of the magnitudes of the amplitudes determined from the following analyses:

(1) The reaction $K^- p \to \varphi\Lambda$ at 4.2 GeV/c[21] (Ref. 22)
(2) The reaction $K^- p \to \varphi\Lambda$ using the combined BNL and EP data (Ref. 23)
(3) The reaction $\pi^- p \to K^{*0}\Lambda$ at 4.5 GeV/c (Ref. 24).
(4) The reaction $\pi^- p \to K^{*0}\Lambda$ at 3.9 GeV/c (Ref. 25)

All these analyses are seen to give remarkably similar results in excellent agreement with the quark model prediction.[26]

The prediction of equality of the amplitudes for $K^- p \to \varphi\Lambda$ and $\pi^- p \to K^{*0}\Lambda$ is also arrived at using SU(3) and factorization on the various t-channel exchange amplitudes (see Table II). Thus it is not clear whether the experimental equality is a success for the quark model or for SU(3) plus factorization. The quark model, however, does not relate $K^- p \to \varphi\Lambda$ to $K^- p \to \omega\Lambda$, whereas SU(3) plus factorization does. From Table II it can be seen that if the K** and K* exchange amplitudes exhibit strong EXD then

$$\rho_n \frac{d\sigma}{dt}(K^- p \to \varphi\Lambda) = 2\rho_n \frac{d\sigma}{dt}(K^- p \to \omega\Lambda) \quad , \qquad (4.3)$$

where the differential cross sections are multiplied by $\rho_n = \rho_{11} + \rho_{1\,-1}$ to project out the natural parity (K**,K*) part. In addition the duality diagram for $K^- p \to \varphi\Lambda$ is planar, whereas $K^- p \to \omega\Lambda$ has a non-planar diagram (assuming ideal mixing for ω and φ). Thus duality diagram arguments predict the (K**,K*) exchange to be purely real for $K^- p \to \omega\Lambda$ and have a rotating phase ($e^{-i\pi\alpha(t)}$) for $K^- p \to \varphi\Lambda$. Equation (4.3) is thus analogous (assuming SU(3)) to the line reversal relation for $K^- n \to \pi^-\Lambda$ and $\pi^- p \to K^0\Lambda$ (2.4a) except here one has the same incident particle (K^-) and hence (4.3) can be tested in the same experiment (this reduces normalization problems). The results for $K^- p \to (\omega,\varphi)\Lambda$ are shown in Fig. 9. The relation (4.3) is seen <u>not</u> to hold and just as occurred in pseudoscalar production (Fig. 1) the "rotating" reaction lies below the "real" reaction. Assuming SU(3) is good, one concludes the EXD of the K** and K* amplitudes is broken in a manner similar to that found in pseudoscalar production. It could be argued for $K^- n \to \pi^-\Lambda$ and $\pi^- p \to K^0\Lambda$ that the distention between "real" and "rotating" is meaningless and that the pion induced reaction is just smaller than the kion induced one. Here, however, both reactions are kion induced and the systematics are the same!

The reactions $K^-n \to \pi^-\Lambda$ and $\pi^-p \to K^0\Lambda$ have large non-zero polarizations produced by the K** and K* exchange amplitudes.[27] If systematics are indeed similar one expects large polarization effects in $K^-p \to (\omega,\varphi)\Lambda$. The Λ polarization in $K^-p \to (\omega,\varphi)\Lambda$ is, however, made up of the two pieces ($P = P_n + P_u$); one arising from the interference between natural parity t-channel amplitudes P_n and one arising from the interference between unnatural parity t-channel amplitudes P_u. By observing the joint correlations between the vector meson and the Λ decay in addition to single density matrix elements and Λ polarization one can determine these two pieces separately.[28] Figure 10 shows the results for $K^-p \to (\omega,\varphi)\Lambda$. It can be seen that the natural parity K** and K* amplitudes do indeed produce a large polarization P_n and that this polarization changes sign in going from ω to φ production. This sign change is predicted by the SU(3) coefficients in Table II. (The K* changes sign under $\omega \to \varphi$ whereas K** does not so $P_n \propto \mathrm{Im}[(K^{**})(K^*)^*]$ does change sign.)

The reactions $K^-p \to (\omega,\varphi)\Lambda$ and $\pi^-p \to K^{*0}\Lambda$ also provide a first look into the nature of unnatural parity Y=1 exchange (i.e., K, K_B, K_A exchange[29]). One striking fact about Fig. 10 is that P_u is not zero. The total polarization P receives a contribution from both natural parity exchange and a contribution from unnatural parity exchange. In particular for $K^-p \to \varphi\Lambda$ P_n and P_u have opposite signs for $|t| \lesssim 0.4$ GeV/c producing a small total polarization, whereas for $K^-p \to \omega\Lambda$ P_n and P_u have the same sign producing very large total polarization. The polarization P_u is made up of two terms[27]

$$P_u \propto \mathrm{Im}[(K)(K_A)^*] + \mathrm{Im}[(K_B)(K_A)^*] \ . \qquad (4.4)$$

The second term changes sign under $\varphi \to \omega$ production, whereas the first term does not (see Table II). In the absence of an amplitude with the quantum numbers of the K_A the polarization P_u would vanish. The experimental data for $K^-p \to (\omega,\varphi)\Lambda$ and also for $\pi^-p \to K^{*0}\Lambda$ seem to indicate the presence of K-K_A interference.[30] Certainly this was not expected.

To this point specific models for the behavior of the amplitudes have not been used. It is necessary, however, if one wants to compare $K^-p \to (\omega,\varphi)\Lambda$ using SU(3) to use a model for the behavior of the K**, K*, K, K_B and K_A exchanges listed in Table II. Figures 11, 12, and 13 show the results of a simple Regge pole fit to the observables for $K^-p \to (\omega,\varphi)\Lambda$ where SU(3) was used to relate the Regge exchanges in $K^-p \to \omega\Lambda$ to those in $K^-p \to \varphi\Lambda$ (Table II). Solution 1 (dashed curves) contains a K**, K*, K, and K_B pole whereas solution 2 (solid curve) also contains a K_A pole.[27] Figures 14 and 15 show the resulting fits to the transversity amplitudes for $K^-p \to (\omega,\varphi)\Lambda$. These effective pole fits illustrate the following points:

(1) Whereas the quark model has no prediction for the relationship between $K^-p \to (\omega,\varphi)\Lambda$, SU(3) successfully explains the relationships between these reactions. It explains the systematics of the relationships between the transversity amplitudes for $K^-p \to (\omega,\varphi)\Lambda$ (Figs. 15 and 16).[31]

(2) Large EXD breaking is required between the K** and K* effective poles. The fits require a K* without wrong signature nonsense α-factors (WSNZ).

(3) One gets a much better fit when a K_A pole is included and P_u is explained primarily by K-K_A interference (Fig. 13) since this quantity does not change sign under $\omega \to \varphi$. Whether one is really seeing an actual K_A pole or effects of Regge-Regge cuts and/or lower lying 1/s effects remains to be seen (studies of the energy dependences of the transversity amplitudes will help settle this point).

The question arises as to why effective K** and K* Regge poles are able to describe the observed natural parity behavior for $K^-p \to (\omega,\varphi)\Lambda$ and $\pi^-p \to K^{*0}\Lambda$ but are inadequate to explain the observables for $K^-n \to \pi^-\Lambda$ and $\pi^-p \to K^0\Lambda$. A possible explanation lies in the nature of absorptive corrections. These corrections tend to be smaller for "flip" type amplitudes (amplitudes vanishing in the forward directions) than for "non-flip" amplitudes (amplitudes peaking in the forward direction). Because the K** and K* couple only to vector meson equal ± 1 states and because of the evasive nature of these poles, all the natural parity (K**,K*) amplitudes behave like "flip" amplitudes in $K^-p \to (\omega,\varphi)\Lambda$ and $\pi^-p \to K^{*0}\Lambda$. For the reactions $K^-n \to \pi^-\Lambda$ and $\pi^-p \to K^0\Lambda$, on the other hand, the K** and K* couple to both a "non-flip" and a "flip" amplitude. This is illustrated by Fig. 1 and Fig. 9 where it can be seen that $d\sigma/dt$ for $K^-n \to \pi^-\Lambda$ and $\pi^-p \to K^0\Lambda$ does not dip in the forward direction, whereas the natural parity contribution to $d\sigma/dt$ for $K^-p \to (\omega,\varphi)\Lambda$ dips in the forward direction. One can understand effective K** and K* poles working for $K^-p \to (\omega,\varphi)\Lambda$ and $\pi^-p \to K^{*0}\Lambda$ because absorptive correction are small for "flip" type amplitudes and not working for $K^-n \to \pi^-\Lambda$ and $\pi^-p \to K^0\Lambda$ because the large non-flip absorptive correction must be included.

V. PHOTOPRODUCTION WITH Y = 1 EXCHANGE

The vector meson dominance model (VDM) relates the amplitudes for the vector meson production reactions $K^-p \to (\rho,\omega,\varphi)\Lambda$ with those of the photoproduction reaction $\gamma p \to K^+\Lambda$ as follows:

$$A(\gamma p \to K^+\Lambda) \propto 3A(\rho p \to K^+\Lambda)+A(\omega p \to K^+\Lambda)-\sqrt{2}\,A(\varphi p \to K^+\Lambda), \tag{5.1}$$

where the ρ, ω, and φ have only ± 1 helicity. The amplitudes $A(\rho p \to K^+\Lambda)$, $A(\omega p \to K^+\Lambda)$, and $A(\varphi p \to K^+\Lambda)$ are related by line reversal to $A(K^-p \to \rho\Lambda)$, $A(K^-p \to \omega\Lambda)$, and $A(K^-p \to \varphi\Lambda)$, respectively. (Note the amplitudes $A(K^-p \to \rho\Lambda)$ and $A(K^-p \to \omega\Lambda)$ are predicted by the quark model or Table II to be equal.) Thus

$$A(\gamma p \to K^+\Lambda) \propto 4[A(K^-p \to \omega\Lambda)]_{l.r.}-\sqrt{2}\,[A(K^-p \to \varphi\Lambda)]_{l.r.}, \tag{5.2}$$

where l.r. means line reversed. Given a model that explains $K^-p \to (\omega,\varphi)\Lambda$ one can use (5.2) to predict the observables for the reaction $\gamma p \to K^+\Lambda$.

Figure 16 shows a comparison of the predicted Λ polarization for $\gamma p \to K^+\Lambda$ from the two Regge pole models of Sec. IV with the experimental values at 5.0 GeV/c.[32] It can be seen that the VDM predictions have the right sign although the magnitude is not as large as observed experimentally. A recent SLAC experiment has measured the polarized photon

asymmetry Σ for $\gamma p \to K^+\Lambda$ and found it to be very large and approximately one for $p_{lab} = 16.0$ GeV/c.[33] The models of Sec. IV also predict this as is also shown in Fig. 16.

VI. SUMMARY AND FUTURE PROJECTS

In this section we present a summary and list interesting future experimental observations.

$K^-n \to \pi^-\Lambda$, $\pi^-p \to K^0\Lambda$ (2 amplitudes)

Using present data on $d\sigma/dt$ and P one can determine two out of the four parameters necessary to completely specify the amplitudes at each s and t. The data indicate that

(1) The K** and K* pole alone are inadequate to describe these reactions. One must include Regge cuts (absorption) corrections and/or lower lying exchanges.

(2) The amplitudes with quantum numbers of the K** and K* do not exhibit EXD. EXD is badly broken.

(3) The line reversal predictions from EXD poles (or duality diagram arguemtns) are badly broken at intermediate energies (3-8 GeV/c).

Interesting future projects include

(1) The determination of line reversal behavior at high energy (> 10 GeV/c). Do the line reversal predictions work better at very high energies?

(2) The determination of the relative phase φ_R. This will allow a complete determination of the production amplitudes (expect overall phase φ_0), but requires a polarized target experiment with a component of the polarization in the production plane (A and R parameters).

$K^-p \to \pi^-Y^{*+}(1385)$ (4 amplitudes)

By observing the two-step decay of the Y*(1385) together with $d\sigma/dt$ one can determine 6 out of the 8 parameters necessary to completely specify the amplitudes at each s and t. The data indicate that

(1) The naive quark model gives a good description of the transversity amplitudes, although the predictions do not hold exactly.

Interesting future projects include

(1) Better statistics so that $\mathrm{Im}\rho^H_{ij}$ can be determined better and tests of duality predictions can be made.

(2) Perform amplitude analysis on $\pi^+p \to K^+Y^{*+}(1385)$[34] or $\pi^-p \to K^0Y^{*+}(1385)$. These reactions are related to $K^-p \to \pi^-Y^{*+}$ (1385) by line reversal and it would be interesting to make a comparison of the amplitudes.

$K^-p \to (\omega,\varphi)\Lambda$, $\pi^-p \to K^{*0}\Lambda$ (6 amplitudes)

By observing the joint correlations between the vector-meson and the Λ-hyperon in addition to the single density matrix elements, Λ polarization, and $d\sigma/dt$, one can determine 10 out of the 12 parameters necessary to completely specify the amplitudes at each s and t. The data indicate that

(1) The quark model (or SU(3)) prediction of equality of the amplitudes for $K^-p \to \varphi\Lambda$ and $\pi^-p \to K^{*0}\Lambda$ works remarkably well.

(2) Using SU(3) one can successfully relate the amplitudes for $K^-p \to \varphi\Lambda$ and $K^-p \to \omega\Lambda$.

(3) The amplitudes with quantum numbers of the K** and K* exchanges do not exhibit EXD and the systematics of this EXD breaking is similar to that found in $K^-n \to \pi^-\Lambda$ and $\pi^-p \to K^0\Lambda$.
(4) The amplitudes with the quantum numbers of the K_A trajectory are not zero at these energies. Whether this is due to an actual K_A pole or Regge-Regge cuts or 1/s effects remains to be seen. In any case, these reactions provide an excellent place to study the unnatural parity exchanges (K, K_A, K_B).

Interesting future projects include

(1) Determination of the energy dependences of the transversity amplitudes. If the unnatural parity exchanges (K, K_B, K_A) lie lower than the natural parity exchanges (K**,K*) we should see the unnatural parity amplitudes die out faster than the natural parity ones.
(2) The determination of the transversity amplitudes for the corresponding Σ production reactions ($K^-p \to (\rho,\omega,\varphi)\Sigma$, $\pi^-p \to K^{*0}\Sigma$). Unnatural parity exchanges should be less important here than in the corresponding Λ reactions.[35] There are several interesting predictions relating the Σ and Λ reactions.[31] For example, is it true that $P_\Sigma = -(P_n)_\Lambda$?
(3) The determination of the relative phase φ_R, which would allow the complete determination of the production amplitudes (except for an overall phase φ_0). This requires a polarized target experiment with a component of polarization in the production plane.

$\gamma p \to K^+\Lambda$ (4 amplitudes)

We find that VDM does not work very well in relating $K^-p \to (\omega,\varphi)\Lambda$ to $\gamma p \to K^+\Lambda$, although the correct sign of P_Λ is predicted and the polarized photon asymmetry (Σ) is predicted to be large and positive as is the case experimentally at 16 GeV/c.[33] Interesting future observations include the determination of the energy dependence of the polarized photon asymmetry. Experimental results indicate that the reaction proceeds via an almost pure natural parity (K**,K*) exchange at 16 GeV/c. It would be interesting to determine the energy dependence of the unnatural parity contributions by measuring Σ at lower energies.

$K^-p \to (\rho,\omega,\varphi)Y^*(1385)$, $\pi^-p \to K^{*0}Y^*(1385)$ (12 amplitudes)

By observing the two-step decay of the Y*(1385) in addition to the vector-meson decay (triple correlations!) and $d\sigma/dt$ one can determine 22 out of the 24 parameters necessary to completely specify the amplitudes at each s and t. There has been no such analysis to date but results should be forthcoming.[36] There are a number of quark model predictions to be tested also SU(3) relationships between $K^-p \to \rho Y^*(1385)$ and $K^-p \to \varphi Y^*(1385)$ and between $K^-p \to \varphi Y^*(1385)$ and $\pi^-p \to K^{*0}Y^*(1385)$.

ACKNOWLEDGMENTS

I would like to thank all my collaborators: M. Aguilar-Benitez, F. Barreiro, A. Rouge, H. Videau, S.U. Chung, and especially Dr. R.L. Eisner. I thank H.A. Gordon, K.-W. Lai, and J.M. Scarr for interesting discussions concerning their results. I also thank Dr. N.P. Samios for his interest and support.

APPENDIX
DEFINITION AND USEFUL RELATIONS FOR TRANSVERSITY AMPLITUDES

The transversity amplitudes for the reaction ab → cd are written as follows:

$$T_{\lambda_c\lambda_d;\lambda_a\lambda_b}(s,t) \quad , \tag{A.1}$$

where $\lambda_a,\lambda_b,\lambda_c$ and λ_d correspond to the components of spin of the particles along the transversity z-axis. The transversity frame is defined with z-axis normal to the production plane (the normal is defined by $\hat{n} = \vec{p}_i \times \vec{p}_f/|\vec{p}_i \times \vec{p}_f|$, where $\vec{p}_i$ and $\vec{p}_f$ are the three momenta of the initial and final meson, respectively). The transversity y-axis is chosen either in the direction of the outgoing particle c (d) as seen in the c.m. frame (helicity-transversity frame) or in the direction of the incoming meson a (b) in the rest frame of the outgoing meson c (d) (Jackson-transversity frame); the x-axis is chosen so as to produce a right-handed coordinate system. Thus the s-channel helicity frame (H) and the helicity-transversity frame (HT) are related by

$$(-x_{HT}, y_{HT}, z_{HT}) = (x_H, z_H, y_H) \quad . \tag{A.2a}$$

Similarly the Jackson frame (J)(t-channel frame) and the Jackson-transversity frame (JT) are related by

$$(-x_{JT}, y_{JT}, z_{JT}) = (x_J, z_J, y_J) \quad , \tag{A.2b}$$

Parity conservation in the production process implies

$$T_{\lambda_c\lambda_d;\lambda_a\lambda_b}(s,t) = \eta_1\eta_2\eta_3^*\eta_4^*(-1)^{\lambda-\mu}T_{\lambda_c\lambda_d;\lambda_a\lambda_b}(s,t) \tag{A.3}$$

where η_i and s_i is the parity and spin of particle i and $\lambda = \lambda_1+\lambda_2$, $\mu = \lambda_3+\lambda_4$. In a given reaction half the transversity amplitudes vanish by parity.

From (A.2) it can be seen that the transversity type frames are related to the helicity type frames by a rotation $R = (\pi/2, \pi/2, \pi/2)$. Thus

$$T_{\lambda_3\lambda_4;\lambda_1\lambda_2}(s,t) = \sum_{\substack{\mu_1\mu_2\mu_3\\ \mu_4}} H_{\mu_3\mu_4;\mu_1\mu_2}(s,t) D^{s_1}_{\mu_1\lambda_1}(R) D^{s_2}_{\mu_2\lambda_2}(R) D^{s_3*}_{\mu_3\lambda_3}(R) D^{s_4*}_{\mu_4\lambda_4}(R) \quad , \tag{A.4}$$

where the amplitudes $T_{\lambda_3\lambda_4;\lambda_1\lambda_2}(s,t)$ correspond to helicity-transversity amplitudes (Jackson-transversity) when $H_{\mu_3\mu_4;\mu_1\mu_2}(s,t)$ are s-(t-) channel helicity amplitudes.

The joint density matrix elements are expressed in terms of the s-(t-) channel helicity amplitudes by the usual formula:

$$\rho^{mm'}_{nn'} = \sum_{\lambda_1\lambda_2} H_{mn;\lambda_1\lambda_2} H^*_{m'n';\lambda_1\lambda_2} \Big/ \Sigma \quad , \qquad \text{(A.5a)}$$

where $\Sigma = \sum_{\lambda_1\lambda_2\lambda_3\lambda_4} |H_{\lambda_3\lambda_4;\lambda_1\lambda_2}|^2$, and where $\rho^{mm'}_{nn'}$ are measured in the s-channel helicity (Jackson) frame. Similarly the joint density matrix elements measured in the transversity frame are related to the transversity amplitudes by

$$T\rho^{mm'}_{nn'} = \sum_{\lambda_1\lambda_2} T_{mm';\lambda_1\lambda_2} T^*_{m'n';\lambda_1\lambda_2} \Big/ \Sigma \quad , \qquad \text{(A.5b)}$$

where

$$\Sigma = \sum_{\lambda_1\lambda_2\lambda_3\lambda_4} |T_{\lambda_3\lambda_4;\lambda_1\lambda_2}|^2 \quad .$$

Single density matrix elements are related to the corresponding joint density matrix elements by

$$\rho_{mm'} = \sum_{\lambda} \rho^{mm'}_{\lambda\lambda} \quad . \qquad \text{(A.6)}$$

From (A.5a), (A.5b), and (A.4) it is easy to derive the relation between $\rho^{mm'}_{nn'}$ and $T\rho^{mm'}_{nn'}$.

Since rotation from the helicity-transversity frame (HT) to the Jackson-transversity frame (JT) corresponds to a rotation about the z-transversity axis, the transversity amplitudes have very simple properties under crossing. Namely,

$$^{HT}T_{\lambda_3\lambda_4;\lambda_1\lambda_2} = \exp[i\lambda_3\chi_3(s,t)+i\lambda_4\chi_4(s,t)-i\lambda_1\chi_1(s,t)-i\lambda_2\chi_2(s,t)] \; {}^{JT}T_{\lambda_3\lambda_4;\lambda_1\lambda_2} \quad , \qquad \text{(A.7)}$$

where $\chi_i(s,t)$ is the s-t crossing angle of particle i.[37] As can be seen, there is only a phase change under crossing. The magnitudes of the transversity amplitudes are invariant under rotation from the helicity-transversity to the Jackson-tranversity frame.

Table I. Various Models for $K^-n \to \pi^-\Lambda$ $(d\sigma/dt, P)$ and $\pi^-p \to K^0\Lambda$ $(d\bar{\sigma}/dt, \bar{P})$

Type of Model	Successful	Comment
(1a) Duality, EXD(K**,K*) poles	No	Predicts $d\sigma/dt = d\bar{\sigma}/dt$, $P = \bar{P} = 0$
(1b) Weak EXD (K**,K*) poles	No	Predicts $d\sigma/dt = d\bar{\sigma}/dt$, $P = -\bar{P}$
(1c) Broken EXD (K**,K*) poles	No	Predicts $P\, d\sigma/dt = -\bar{P}\, d\bar{\sigma}/dt$
(2a) EXD (K**,K*) poles plus "old" absorption	No	Predicts $d\bar{\sigma}/dt > d\sigma/dt$
(2b) EXD (K**,K*) poles plus "old" absorption plus daughters	Yes	Predicts $d\sigma/dt \to d\bar{\sigma}/dt$ as $s \to \infty$
(2c) EXD (K**,K*) poles plus phenomenological absorption	Yes	somewhat ad hoc
(2d) EXD (K**,K*) poles plus T_{eff} absorption	Yes	little predictive power
(3a) Non-EXD (K**,K*) poles (no WSNZ) plus strong absorption (SCRAM)	Yes	fails elsewhere (i.e., $\pi^-p \to \pi^0n$)
(3b) Non-EXD (K**,K*) poles (no WSNZ) plus "fancy Pomeron" absorption	Yes	more parameters since EXD is abandoned.

Table II. SU(3) Clebsch-Gordon Coefficients for the Reactions $K^-p \to (\omega,\varphi)\Lambda$ and $\pi^-p \to K^{*0}\Lambda$

Exchange	Type Coupling	$K^-p \to \omega\Lambda$	$K^-p \to \varphi\Lambda$	$\pi^-p \to K^{*0}\Lambda$
K**	F-type	1	$\sqrt{2}$	$-\sqrt{2}$
K*	D-type	-1	$\sqrt{2}$	$-\sqrt{2}$
K	F-type	1	$\sqrt{2}$	$-\sqrt{2}$
K_B	D-type	-1	$\sqrt{2}$	$-\sqrt{2}$
K_A	F-type	1	$\sqrt{2}$	$-\sqrt{2}$

FIGURE CAPTIONS

1. Experimental differential cross sections for the reaction $K^-n \to \pi^-\Lambda$ at 3.9 GeV/c (Ref. 38) and the line reversed reaction $\pi^-p \to K^0\Lambda$ at 3.9 GeV/c (Ref. 39). Duality diagrams arguments (or EXD) predict the amplitudes for $K^-n \to \pi^-\Lambda$ be purely real ("real") and those for $\pi^-p \to K^0\Lambda$ to have a rotating ("rotating") phase ($e^{-i\pi\alpha(t)}$).

2. Experimental values of the Λ polarization P and magnitudes of the transversity amplitudes (normalized $|T_{++}|^2+|T_{--}|^2 = 1$) for the reaction $K^-n \to \pi^-\Lambda$ at 3.0 GeV/c (Ref. 40, circles) and 3.9 GeV/c (Ref. 38, triangles) and for the line reversed reaction $\pi^-p \to K^0\Lambda$ at 3.9 GeV/c (Ref. 39, triangles) and 4.5 GeV/c (Ref. 24, circles).

3. Transversity amplitudes and transversity density matrix elements for the reaction $K^-p \to \pi^-Y^{*+}(1385)$,[18] where δ_1 (δ_2) is the relative phase between $T_{3\,-1}$ and $T_{-1\,-1}$ (T_{11} and $T_{-3\,1}$). The quark model predicts $T_{3\,-1} = T_{-3\,1} = 0$ and $T_{11} = T_{-1\,-1} = 1/2$.

4. (A) Illustrates how T_{11} can be represented as a sum of quark-quark scattering amplitudes. The $\pm$ signs represent quark spin projections on the transversity z-axis (normal to production plane).
(B) Illustrates how $T_{3\,-1}$ requires that more than one of the baryon quarks flip sign. The quark model thus predicts that this amplitude vanish.

5. The s-channel helicity density matrix elements for the reaction $K^-p \to \pi^-Y^{*+}(1385)$.[18] The quark model predicts that $\rho^H_{33} = 3/8$, $\mathrm{Re}\rho^H_{3\,-1} = \sqrt{3}/8$, and that the remaining elements vanish.

6. Magnitudes of the transversity amplitudes for the reactions $K^-p \to (\omega,\varphi)\Lambda$. The triangles are the combined 3.9 and 4.6 GeV/c BNL data (Ref. 22) and the circles are combined BNL and Ecole Polytechnique data (Ref. 23).

7. Relative phases of the transversity amplitudes, where $\theta^{\pm 1}_{\pm} = \mathrm{Arg}(T^{\pm\ 1}_{\pm\ \pm}) - \mathrm{Arg}(T^{\ 0}_{\pm\ \pm})$. The data are the same as Fig. 6.

8. Comparison of the amplitudes for $K^-p \to \varphi\Lambda$ using the BNL data (Ref. 22, open circles) and the BNL + EP data (Ref. 23, open triangles) with the amplitudes for $\pi^-p \to K^{*0}\Lambda$ at 3.9 GeV/c Ref. 25, solid triangles) and at 4.5 GeV/c (Ref. 24, solid circles). The quark model predicts equality of the amplitudes for these two reactions.

9. The natural parity ($\rho_n = \rho_{11}+\rho_{1\,-1}$), unnatural parity $\rho_u = \rho_{11}-\rho_{-1\,-1}$), and the total differential cross section for reaction $K^-p \to \varphi\Lambda$ and twice the reaction $K^-p \to \omega\Lambda$. The data are from Ref. 23. EXD plus SU(3) predicts the amplitudes for the natural parity part of the reaction $K^-p \to \omega\Lambda$ be purely real and those for $K^-p \to \varphi\Lambda$ have a rotating phase ($e^{-i\pi\alpha(t)}$).

FIGURE CAPTIONS (cont'd)

10. The natural parity polarization (P_n), unnatural parity polarization (P_u), and total polarization ($P = P_n + P_u$) for the reactions $K^-p \to (\omega,\varphi)\Lambda$ from Ref. 23.

11. Shows an effective Regge pole plus SU(3) fit to the natural parity (ρ_n), unnatural parity (ρ_u) and total differential cross sections for $K^-p \to \varphi\Lambda$ and twice $K^-p \to \omega\Lambda$. The dashed curves are from a model that includes a K**, K*, K, and K_B effective pole, whereas the solid curves are from a model that also includes a K_A effective pole. SU(3) is used to relate the two reactions. The data are from Ref. 23.

12. Shows an effective Regge pole plus SU(3) fit to the single density matrix elements in the helicity frame for $K^-p \to (\omega,\varphi)\Lambda$, where $\rho^H_{\pm} = \rho^H_{11} \pm \rho^H_{1-1}$. The dashed curves are from a model that includes a $\bar{K}$**, K*, K, and K_B effective pole, whereas the solid curves are from a model that also includes a K_A effective pole. SU(3) is used to relate the two reactions. The data are from Ref. 23.

13. Shows an effective Regge pole plus SU(3) fit to the natural parity polarization (P_n), unnatural parity polarization (P_u), and the total polarization ($P = P_n + P_u$). The solid and dashed curves are the two models in Fig. 11 and Fig. 12. The data are from Ref. 23.

14. Comparison of the predictions of the two effective pole plus SU(3) models shown in Figs. 11, 12, and 13 with the experimentally determined transversity amplitudes of Fig. 6.

15. Comparison of the predictions of the two effective pole plus SU(3) models shown in Figs. 11, 12, and 13 with the relative phases of Fig. 7.

16. Shows the predictions of the two effective pole plus SU(3) models shown in Figs. 11, 12, and 13 for the Λ polarization (P) and polarized photon asymmetry (Σ) for the reaction $\gamma p \to K^+\Lambda$, where VDM is used to relate the photon to the vector mesons ρ, ω, and φ. The data are Λ polarization at 5.0 GeV/c from Ref. 32.

REFERENCES

1. A.D. Martin, Proceedings of the Seventh Rencontre de Moriond (1972) ed. J. Tran Thanh Van.
2. H. Harari, Phys. Rev. Letters 22, 562 (1969); J.L. Rosner, Phys. Rev. Letters 22, 689 (1969).
3. R.D. Field and J.D. Jackson, Phys. Rev. D4, 693 (1971).
4. A. Krzywicki and J. Tran Thanh Van, Phys. Letters 30B, 185 (1969).
5. A.C. Irving, A.D. Martin and C. Michael, Nucl. Phys. B32, 1 (1971).
6. N.J. Sopkovich, Nuovo Cimento 26, 186 (1962); K. Gottfried and J.D. Jackson, Nuovo Cimento 34, 735 (1964).
7. R.D. Field, Phys. Rev. D5, 86 (1972).
8. G.A. Ringland, R.G. Roberts, D.P. Roy and J. Tran Thanh Van, Nucl. Phys. B44, 395 (1972).
9. R.L. Thews, G.R. Goldstein and J.F. Owens, "A New Regge Absorption Model," University of Arizona preprint (1972).
10. D. Barkai and K.J.M. Moriarty, Nucl. Phys. B50, 354 (1972).
11. A. Martin and P.R. Stevens, Phys. Rev. D5, 147 (1972).
12. B. Sadoulet, Nucl. Phys. B (to be published).
13. V. Barger and A.D. Martin, Phys. Letters 39B, 379 (1972).
14. F. Henyey, G.L. Kane, J. Pumplin and M.H. Ross, Phys. Rev. 182, 1579 (1969); M. Ross, F.S. Henyey and G.L. Kane, Nucl. Phys. B23, 269 (1970).
15. R.D. Field, Lawrence Berkeley Laboratory, Report No. LBL-33 (1971) (unpublished).
16. B.J. Hartley and G.L. Kane (preprint).
17. J.S. Loos and J.A.J. Matthews, Phys. Rev. D6, 2467 (1972) have successfuly fit the hypercharge exchange reactions $K^-n \to \pi^-\Lambda$ and $\pi^-p \to K^0\Lambda$ using a dual absorptive type model (DAM). They must, however, make assumptions concerning the behavior of the real parts of the helicity amplitudes since DAM predicts the behavior of the imaginary parts only for K** and K* exchange.
18. M. Aguilar-Benitez, S.U. Chung, R.L. Eisner and R.D. Field, Phys. Rev. Letters 29, 749 (1972).
19. A. Bialas and K. Zalewski, Nucl. Phys. B6, 449 (1968); ibid B6, 465 (1968); ibid B6, 478 (1968).
20. N. Byers and C.N. Yang, Phys. Rev. 135, B796 (1964).
21. We have combined data at 3.9 and 4.6 GeV/c and labelled it 4.2 GeV/c.
22. R.D. Field, R.L. Eisner, S.U. Chung and M. Aguilar-Benitez, Phys. Rev. D (to be published).
23. R.D. Field, R.L. Eisner, A. Rouge, H. Videau, M. Aguilar-Benitez, and F. Barreiro (to be published). We have combined the BNL data of Ref. 22 with Ecole Polytechnique data.
24. D. Crennell, H. Gordon, K.-W. Lai and J.M. Scarr, Phys. Rev. D6, 1220 (1972).
25. M. Abramovich, A.C. Irving, A.D. Martin and C. Michael, Phys. Letters 39B, 353 (1972).
26. The $A^{\pm}_{\mp}$, $B^{\pm}_{\mp}$, and $C^{\pm}_{\mp}$ amplitudes defined here are related to the amplitudes of Ref. 25 by $A^{\pm}_{\mp} = -c_{\pm}$, $B^{\pm}_{\mp} = \mp i a_{\pm}$, $C^{\pm}_{\mp} = \mp b_{\pm}$; and to the amplitudes of Ref. 24 by $A^{\pm}_{\mp} = S_{\pm}$, $B^{\pm}_{\mp} = \mp D_{\mp}$, and $C^{\pm}_{\mp} = \mp A_{\mp}$.

27. These poles are to be understood as "effective" poles into which the effects of Regge cuts and/or lower lying poles have been absorbed.
28. Having determined the amplitudes $A^{\pm}$, $B^{\pm}$, and $C^{\pm}$ it is an easy matter to calculate P_n and P_u. Namely, $P_n = (|A^+|^2 - |A^-|^2)/\Sigma$, $P_u = (|B^-|^2 - |B^+|^2 + |C^-|^2 - |C^+|^2)/\Sigma$ where $\Sigma = |A^+|^2 + |A^-|^2 + |B^+|^2 + |B^-|^2 + |C^+|^2 + |C^-|^2$.
29. The K_B is the $Y = \pm 1$ member of the octet to which the B meson belongs and the K_A is the $Y = \pm 1$ member of the octet to which the A_1 meson belongs.
30. To date there has been no evidence for the necessity of A_1 exchange in $\pi^- p \to \rho^0 n$. However, the question of the importance of A_1 exchange will not be answered until polarized proton target information is used to detect possible π-A_1 interference in $\pi^- p \to \rho^0 n$. Even if future experimental information substantiates the necessity of K_A exchange in $K^- p \to (\omega,\varphi)\Lambda$ and $\pi^- p \to K^{*0}\Lambda$ this would not necessarily imply that the A_1 is important in $\pi^- p \to \rho^0 n$. This would depend on the F/D ratio of the A_1-K_A octet.
31. One can successfully fit the observables for the vector meson production with $Y = 1$ reactions $K^- p \to (\rho,\omega,\varphi)(\Lambda,\Sigma)$ and $\pi^- p \to K^{*0}(\Lambda,\Sigma)$. See, R.D. Field, R.L. Eisner, and M. Aguilar-Benitez, Phys. Rev. D6, 1863 (1972).
32. G. Vogel, H. Burfeindt, G. Buschhorn, P. Heide, U. Kötz, K.-H. Mess, P. Schmuser, B. Sonne and B.H. Wilk, Phys. Letters 40B, 513 (1972).
33. R.H. Siemann (private communication).
34. Quark model predictions appear to be reasonably well satisfied for $\pi^+ p \to K^+ Y^{*+}(1385)$ at 8 GeV/c, although statistics are limited. J.V. Beaupre, H. Grässler, R. Speth, K.-F. Albrecht, M. Walter, G.T. Jones, V. Karimaki, W. Kottel, D. Sotiriou, R. Stroynowski, D. Kisielewska, P. Malecki, J. Zaorska, W. Zielinski, P.J. Dornan, R. Kumas, G. Otter, P. Schmid, H. Piotrowska, and R. Sosnowski, Nucl. Phys. B49, 405 (1972).
35. This is primarily due to the fact that $g^2_{NK\Sigma} \ll g^2_{NK\Lambda}$.
36. R.L. Eisner and M. Aguilar-Benitez (private communication).
37. See Ref. 31 for definitions of the crossing angles.
38. D.J. Crennell, Uri Karshon, Kwan Wu Lai, J.S. O'Neall, J.M. Scarr, R.M. Lea, T.G. Schumann and E.M. Urvator, Phys. Rev. Letters 23, 1347 (1969).
39. M. Abramovitch, H. Blumenfeld, V. Chaloupka, S.U. Chung, J. Diaz, L. Montanet, J. Pernego, S. Reucroft, J. Rubio and B. Sadoulet, Nucl. Phys. B27, 477 (1971).
40. R. Barloutaud, Duong Nhu Hoa, J. Griselin, D.W. Merrill, J.C. Scheuer, W. Hoogland, J.C. Kluyver, A. Minguzzi-Ranzi, A.M. Rossi, B. Haber, E. Hirsch, J. Goldberg and M. Laloum, Nucl. Phys. B9, 493 (1969).

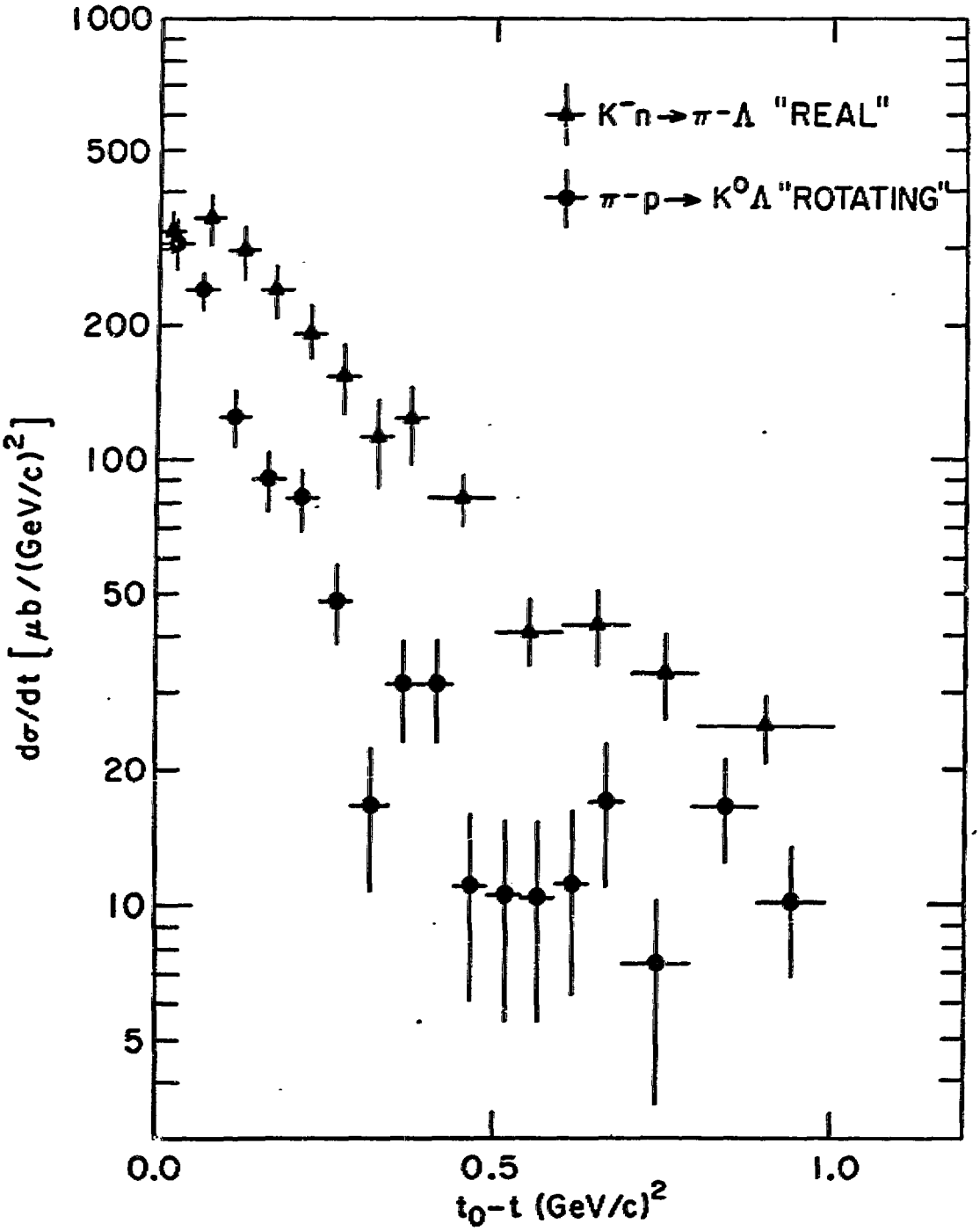

Neg. # 3-449-73

FIGURE 1

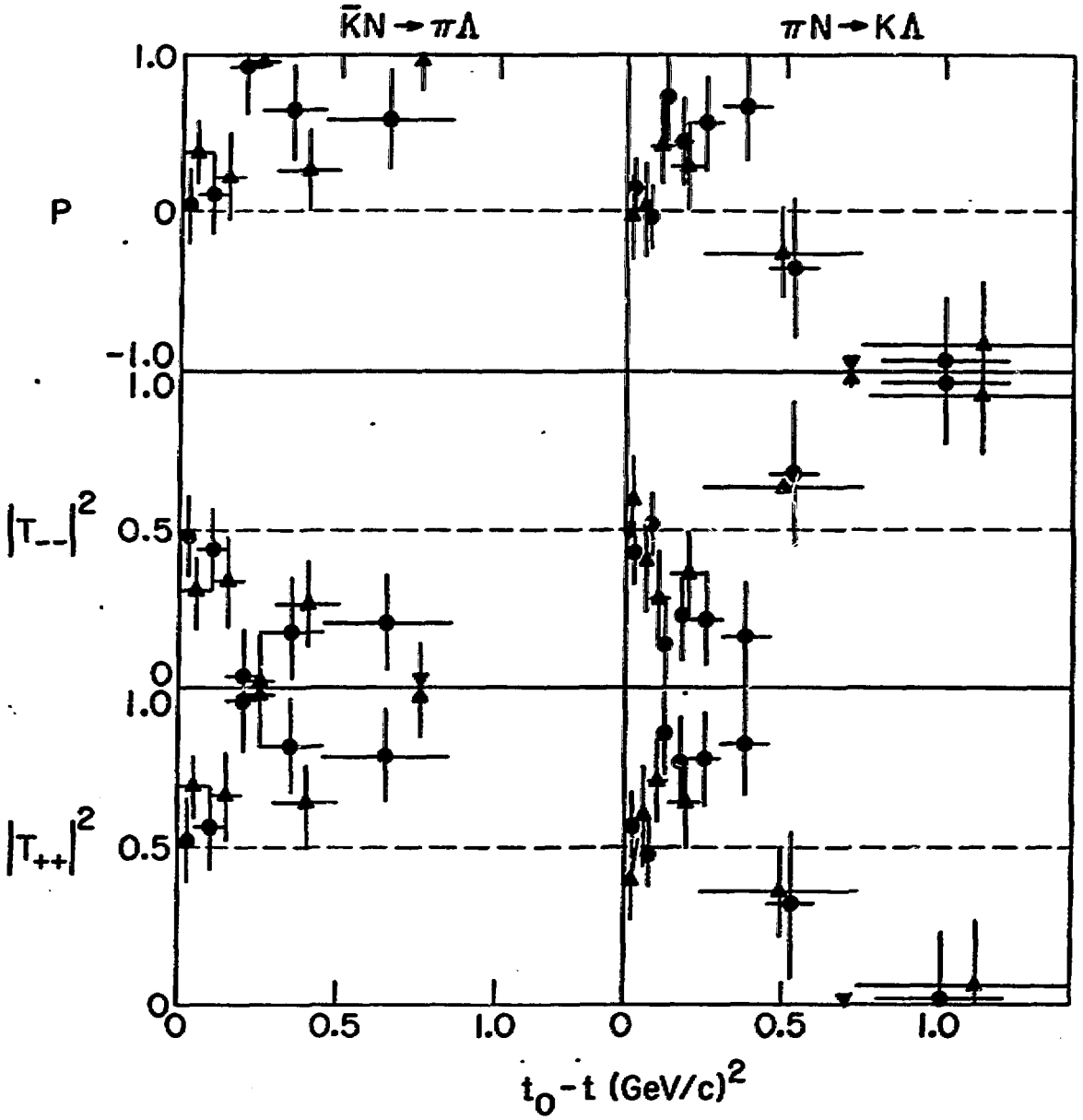

Neg. # 3-24-73

FIGURE 2

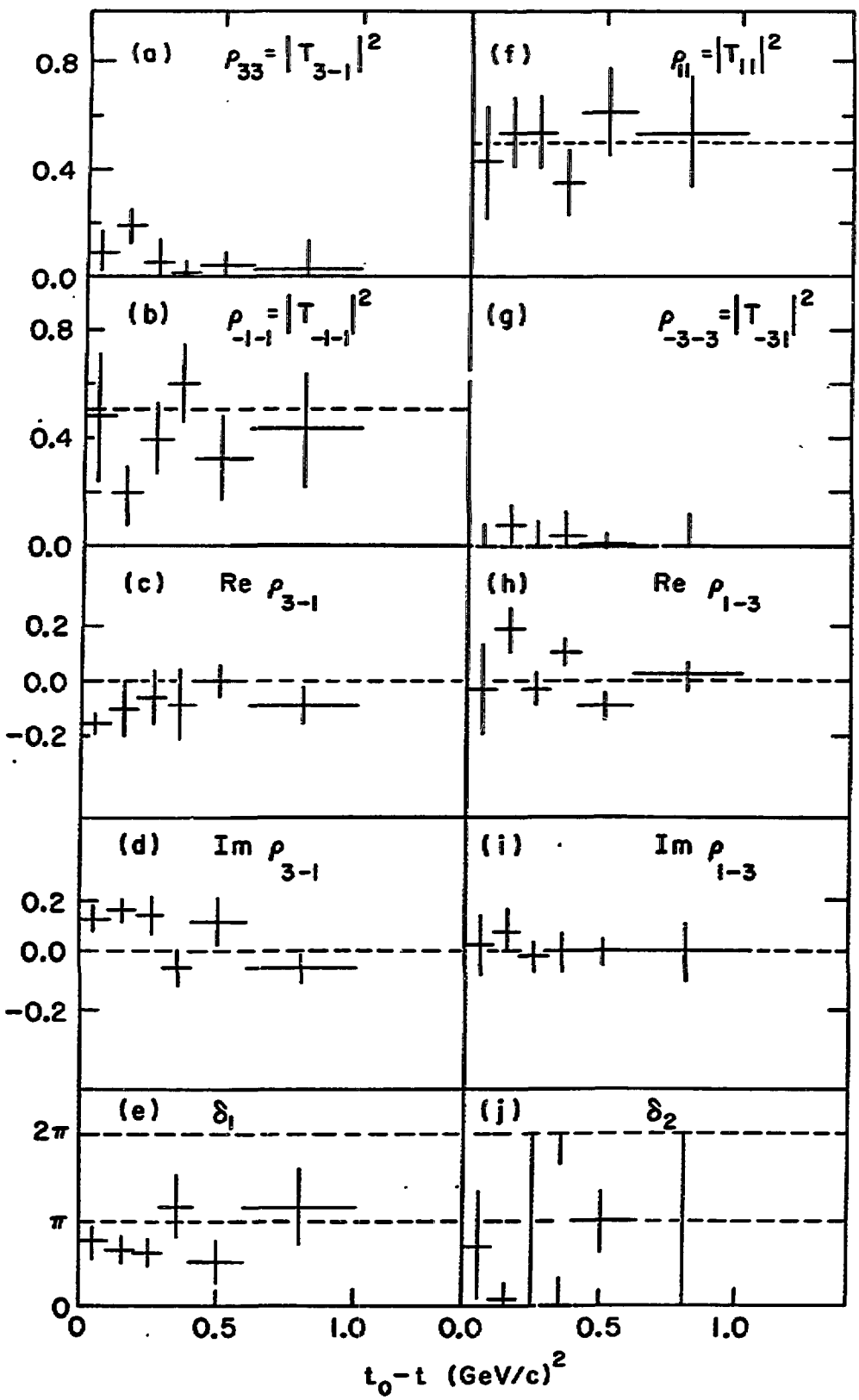

Neg. # 6-512=72

FIGURE 3

(A) $T_{1/2;1/2}(s,t) =$ 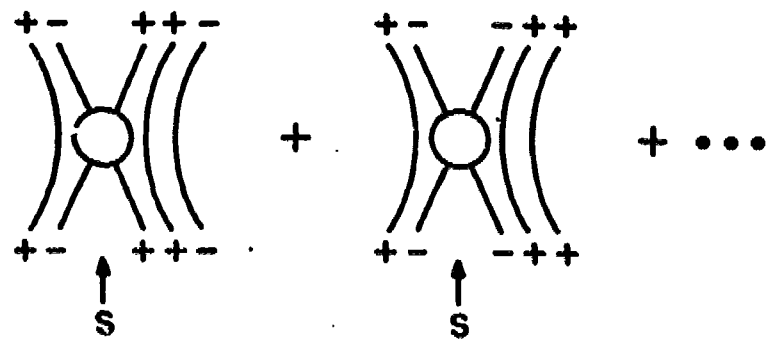

$+ \cdots$

(B) $T_{3/2;-1/2}(s,t) =$ 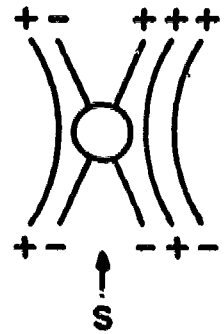

$= 0$

FIGURE 4

Neg. # 4-401-73

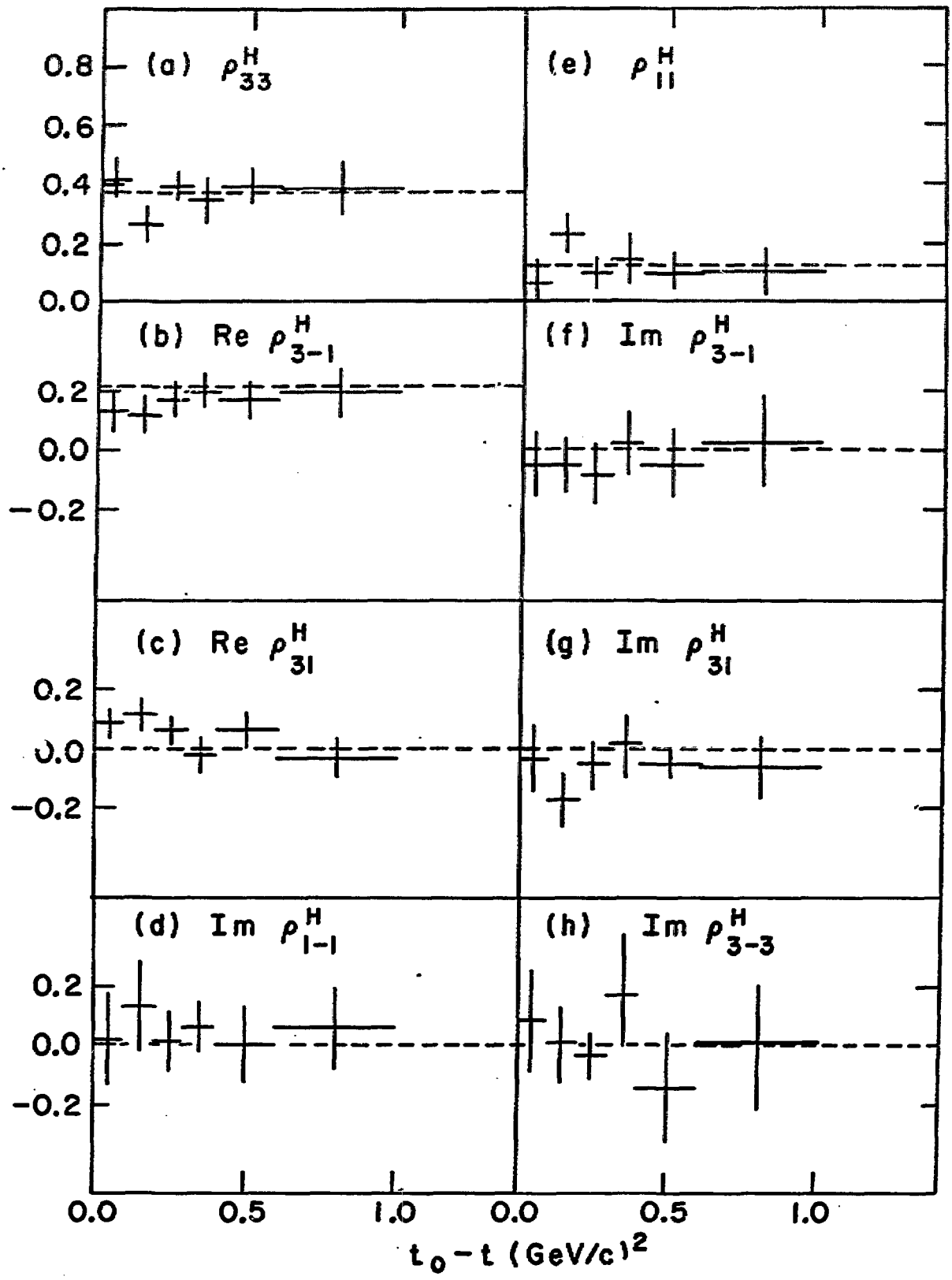

Neg. # 6-513-72

FIGURE 5

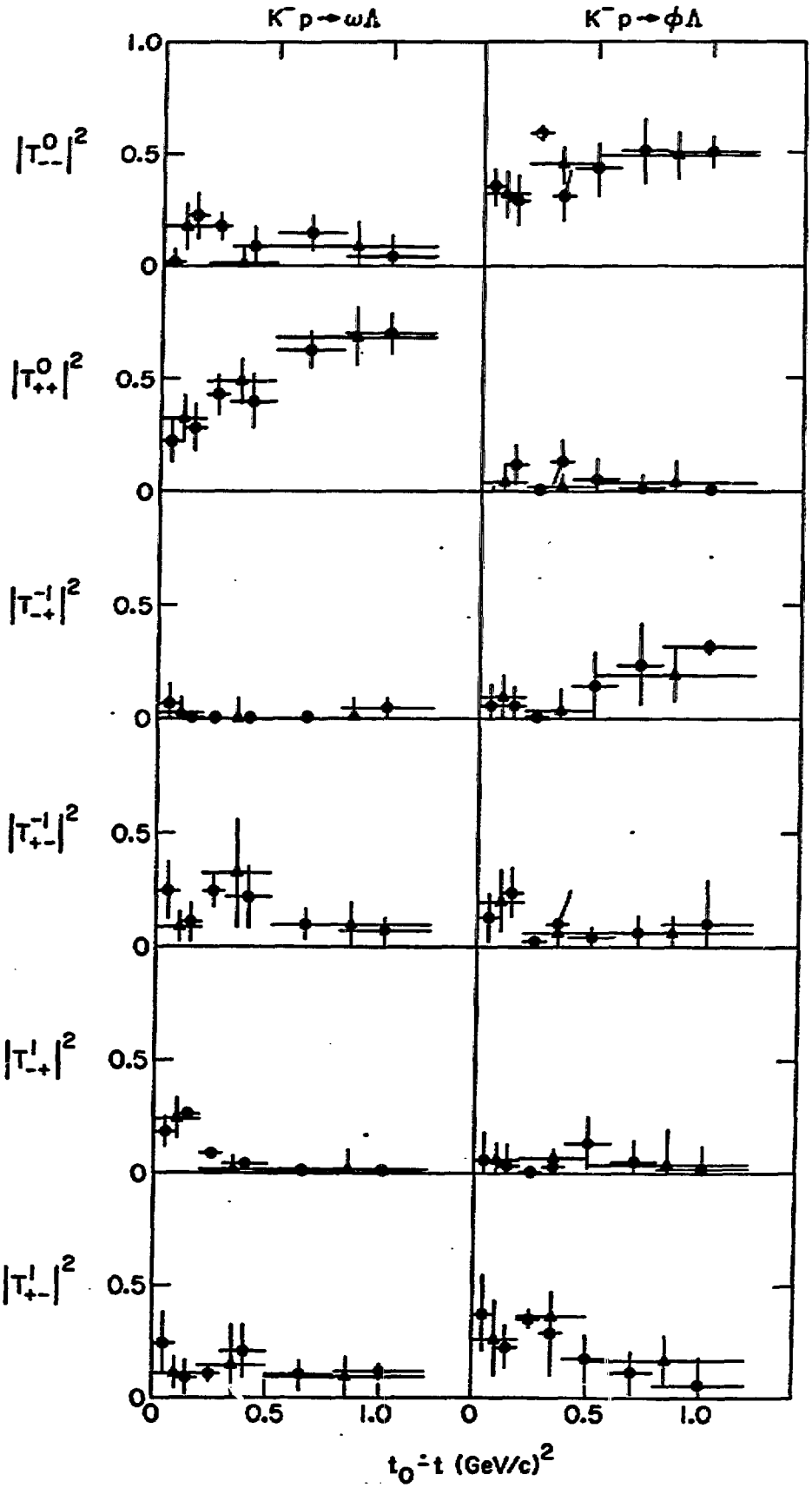

Neg. # 3-28-73

FIGURE 6

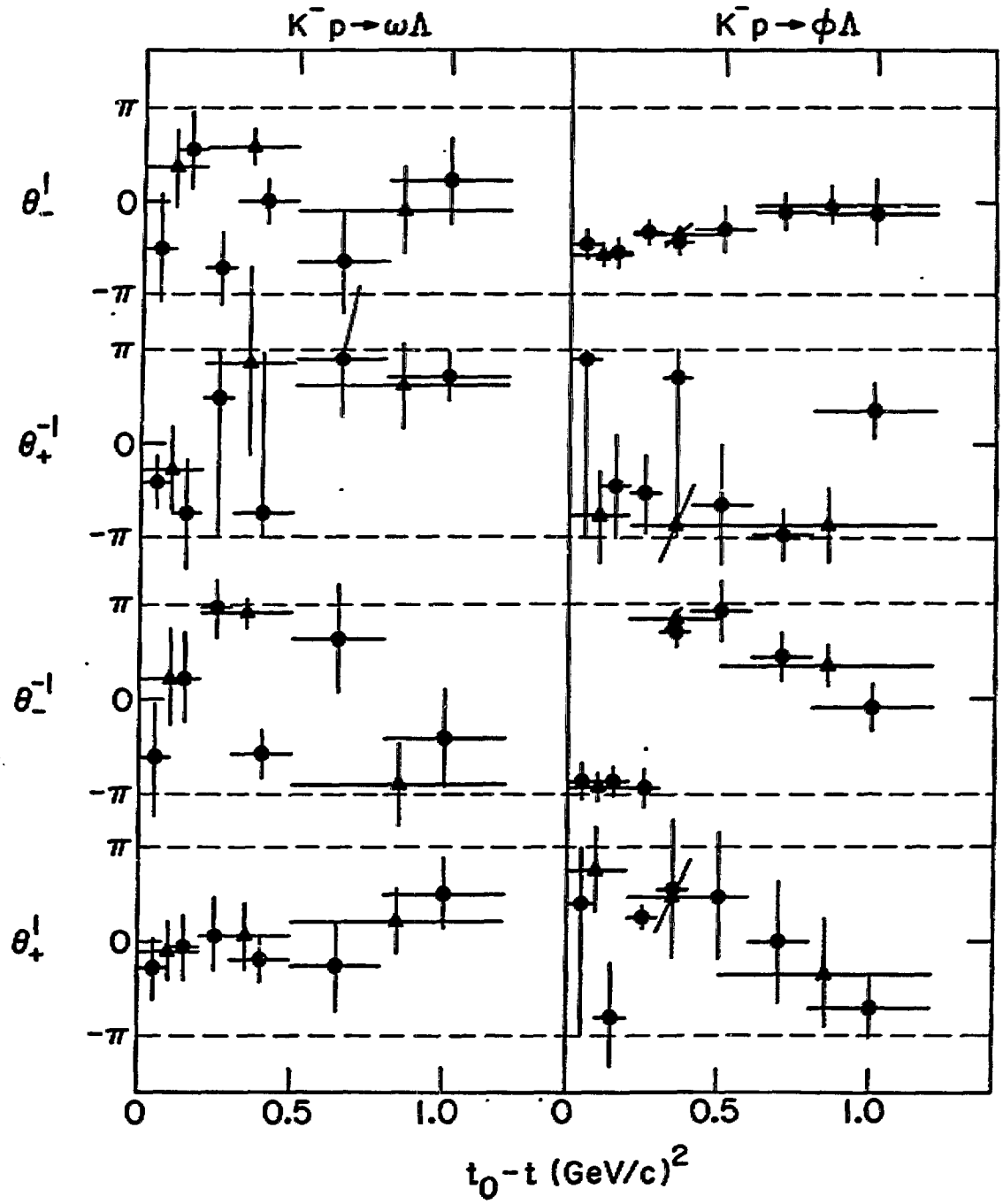

Neg. # 3-23-73

FIGURE 7

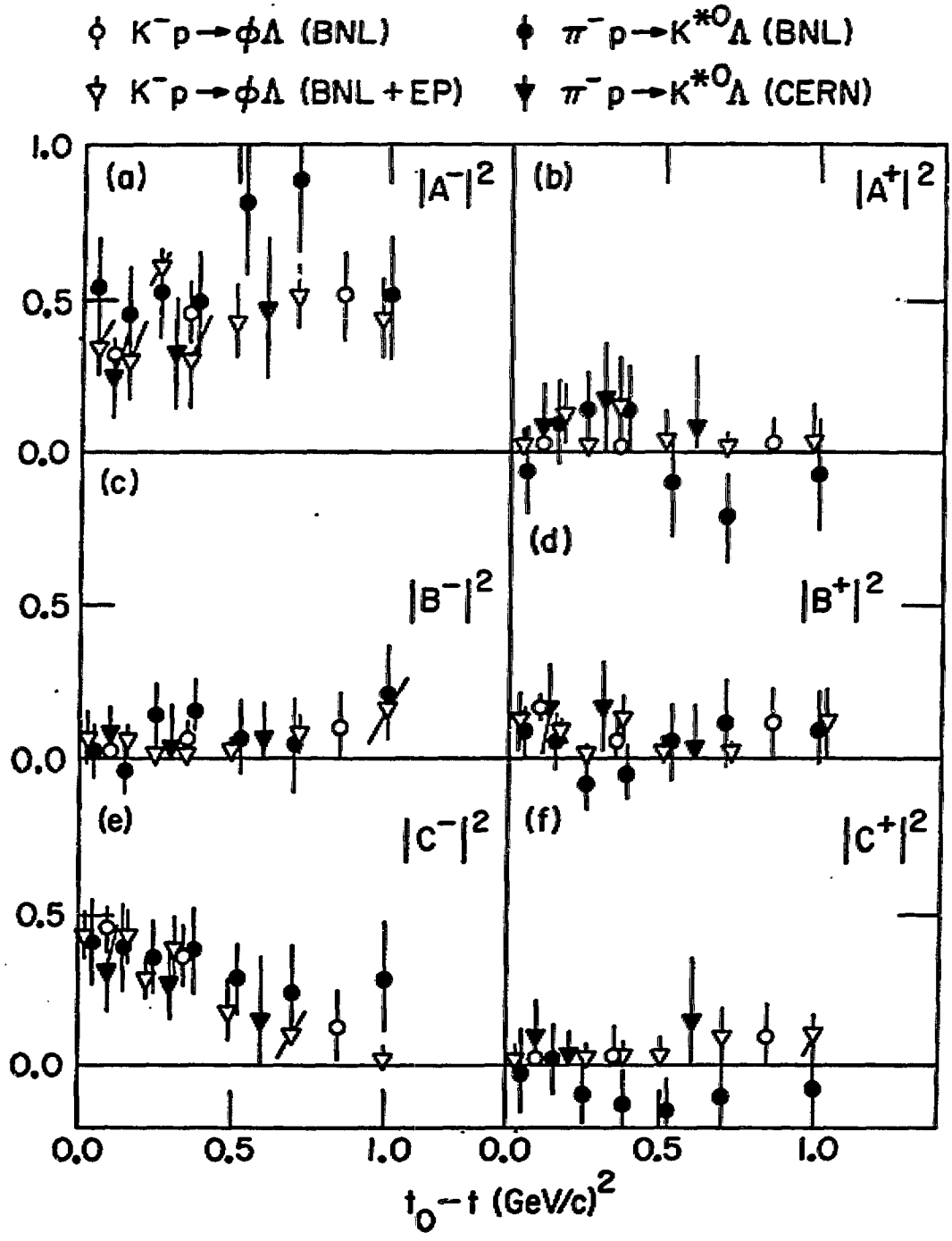

Neg. # 3-26-73

FIGURE 8

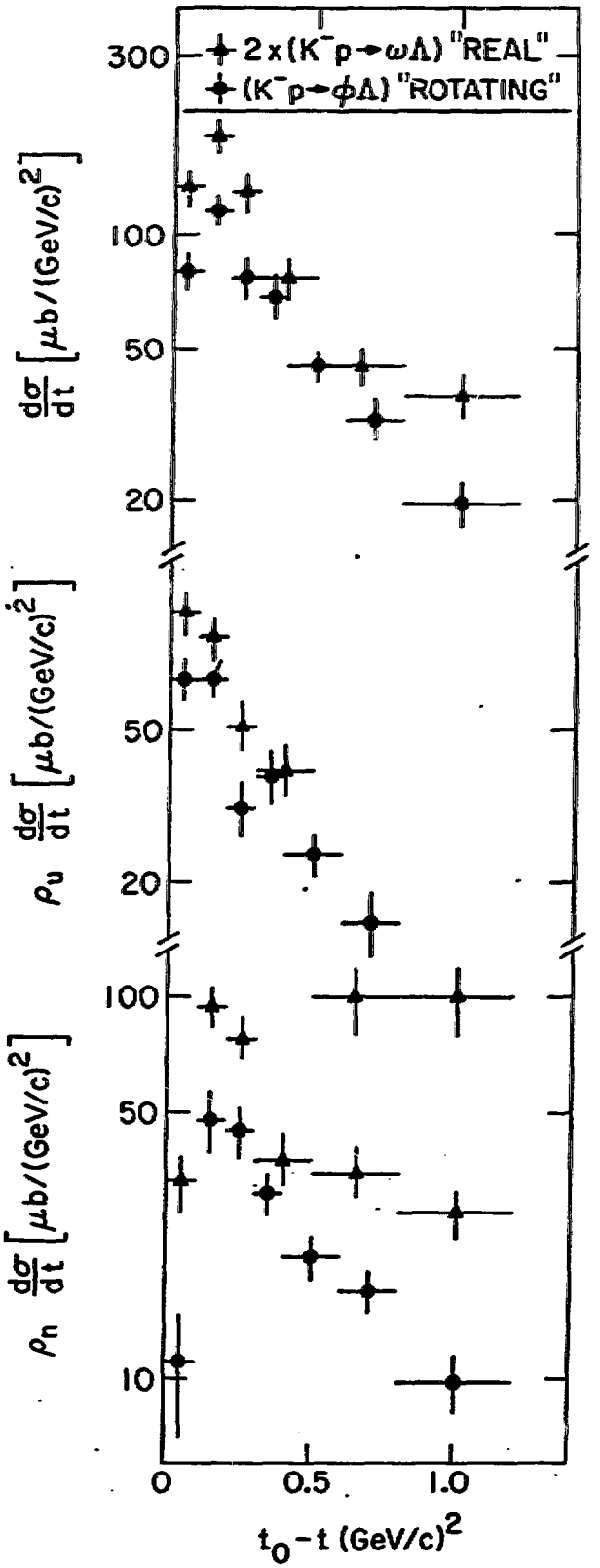

Neg. # 3-27-73

FIGURE 9

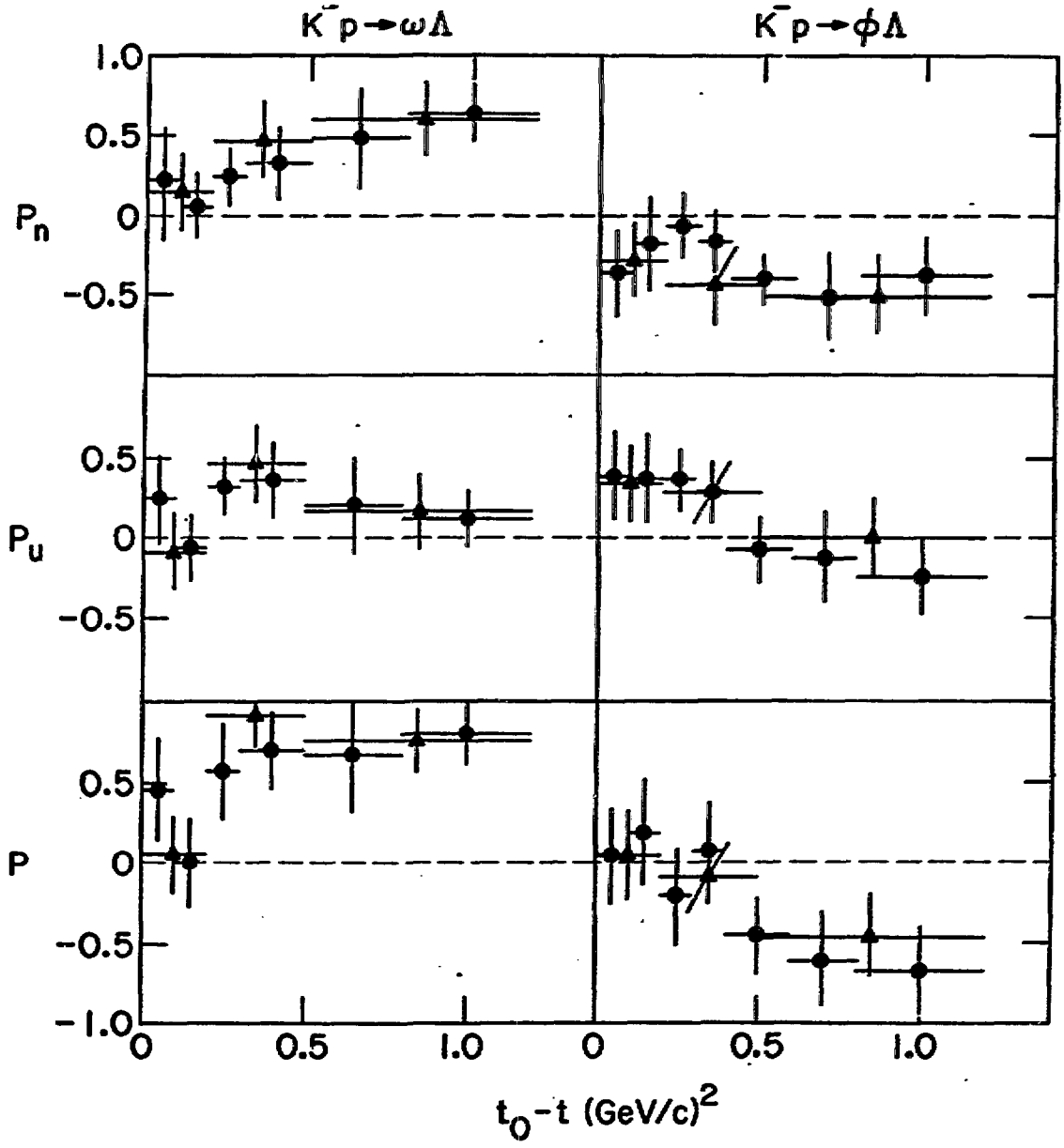

Neg. # 3-22-73

FIGURE 10

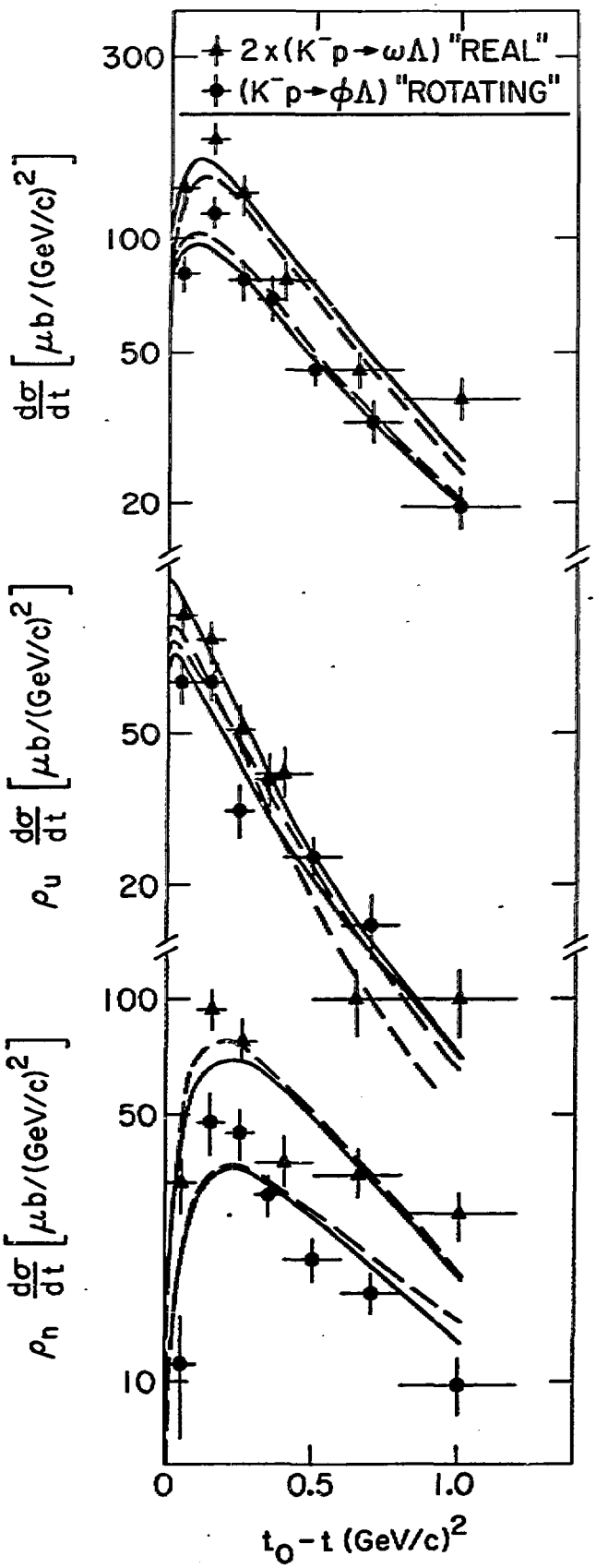

Neg. # 3-617-73

FIGURE 11

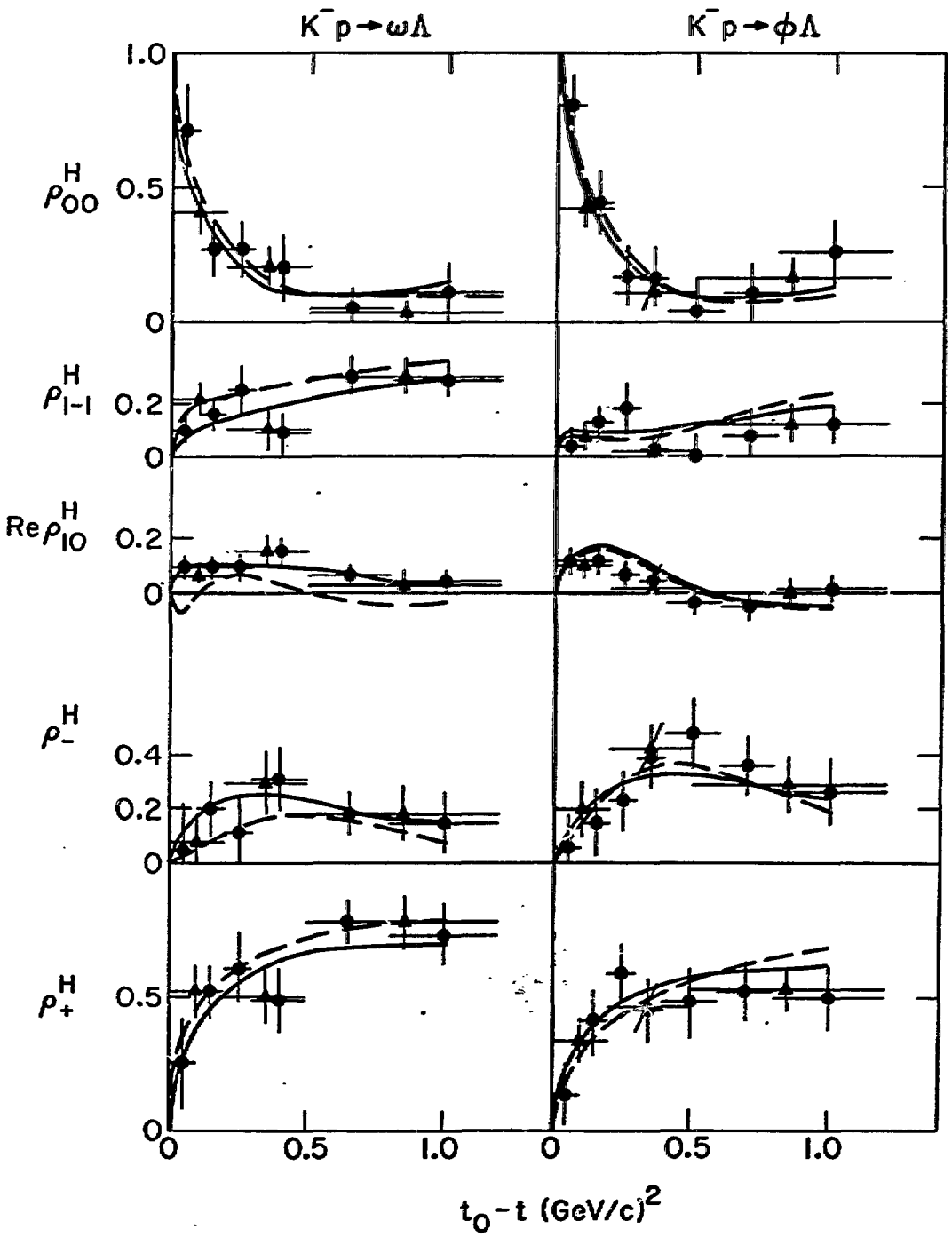

Neg. # 3-618-73

FIGURE 12

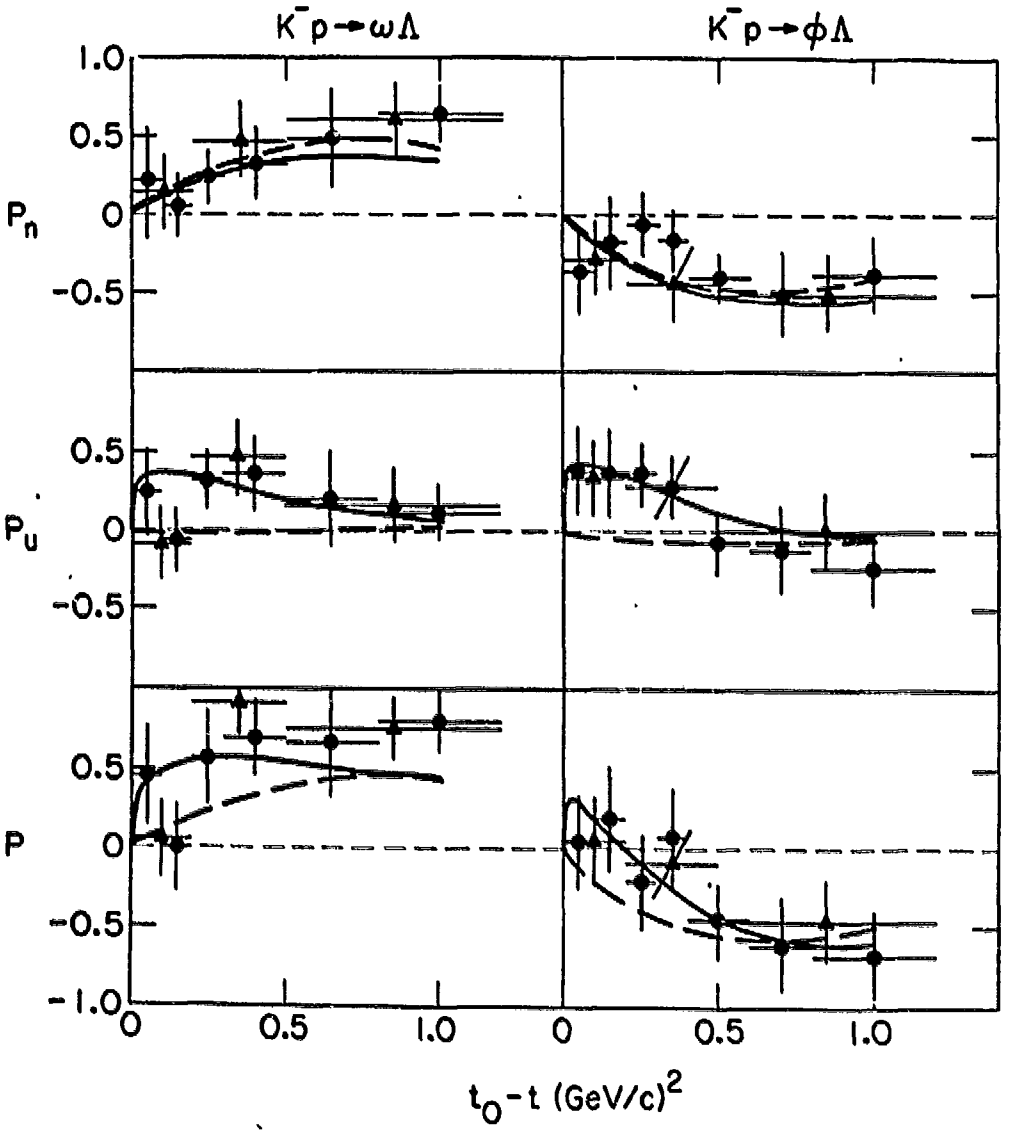

FIGURE 13

Neg. # 3-616-73

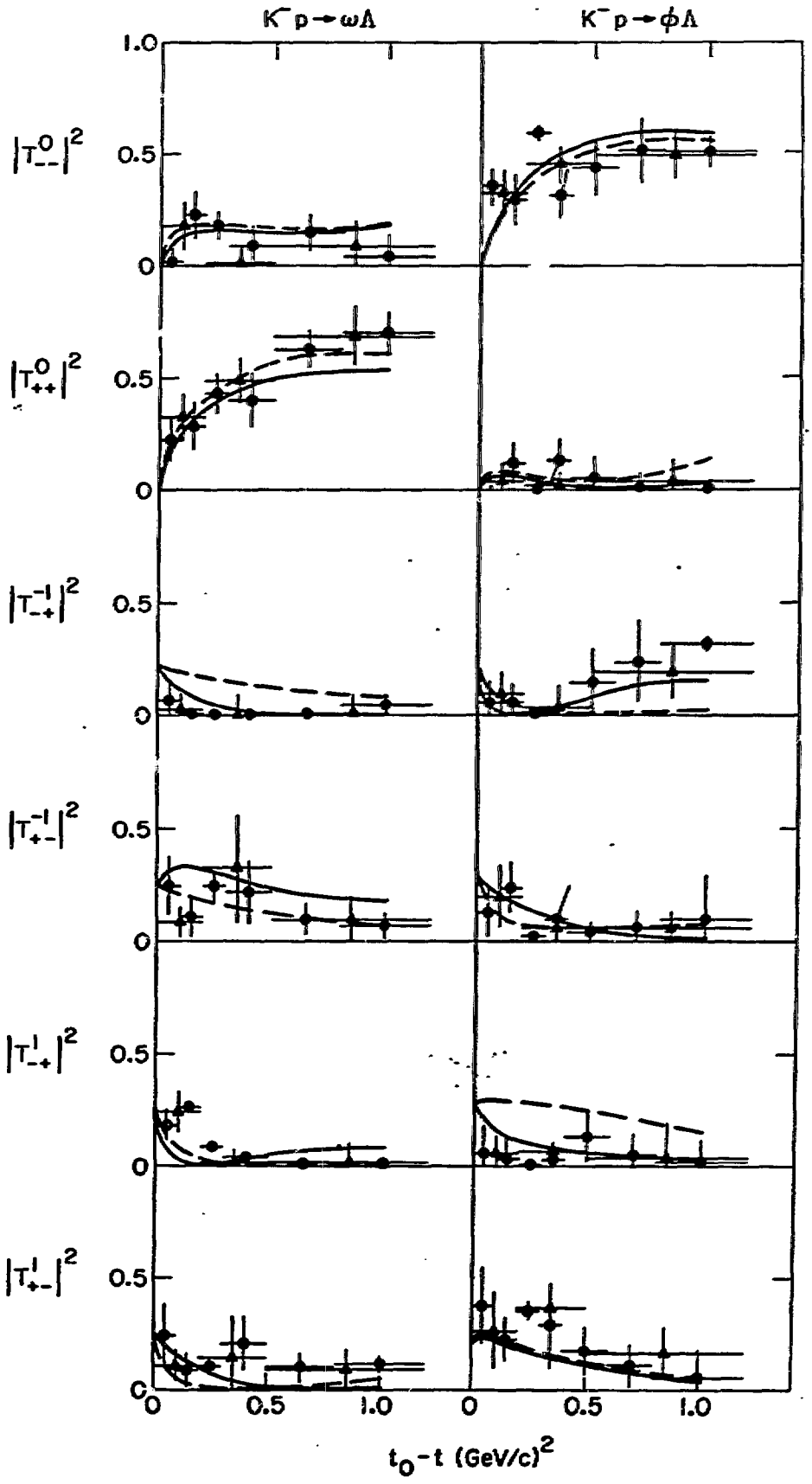

Neg. # 3-619-73

FIGURE 14

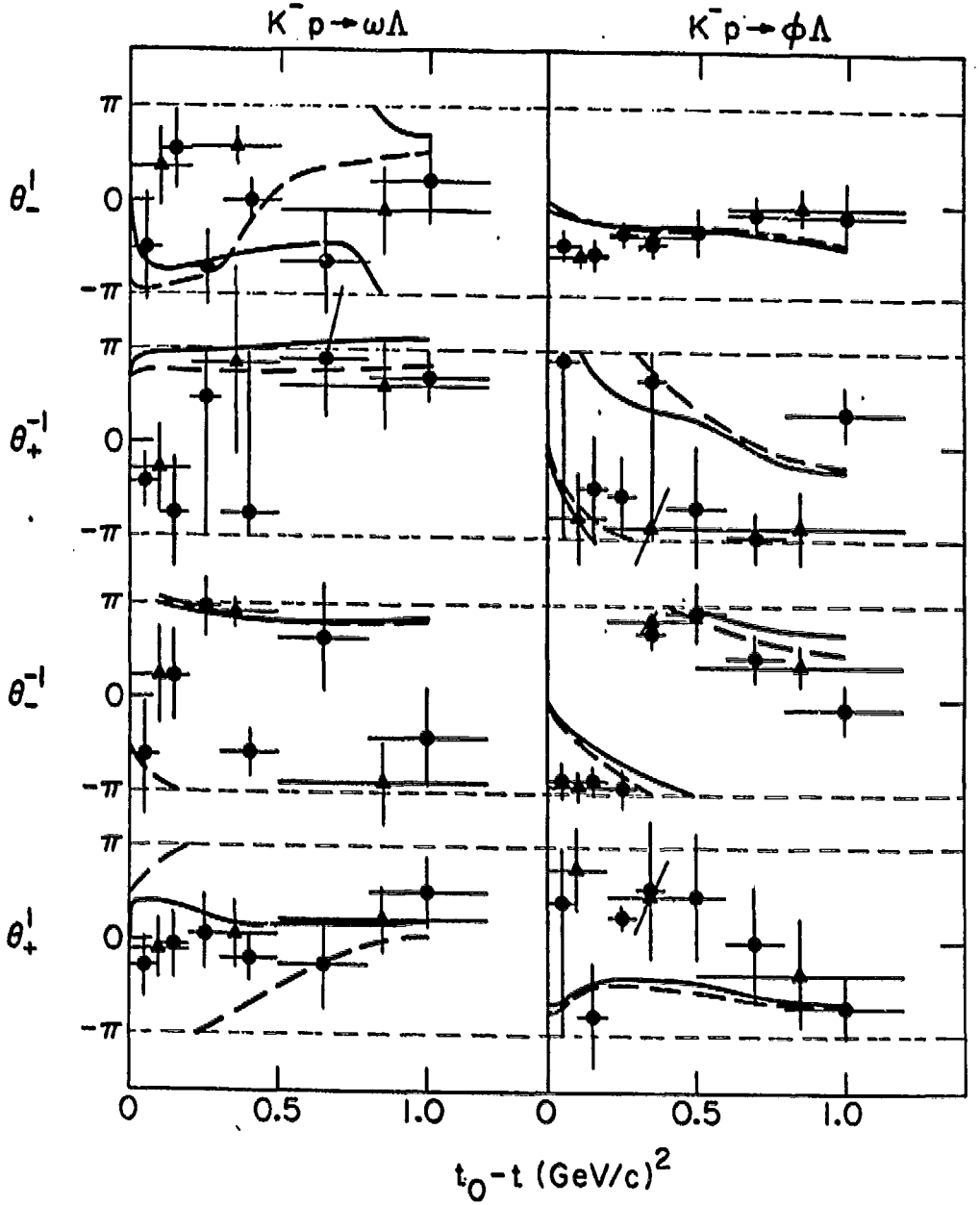

Neg. # 3-616-73

FIGURE 15

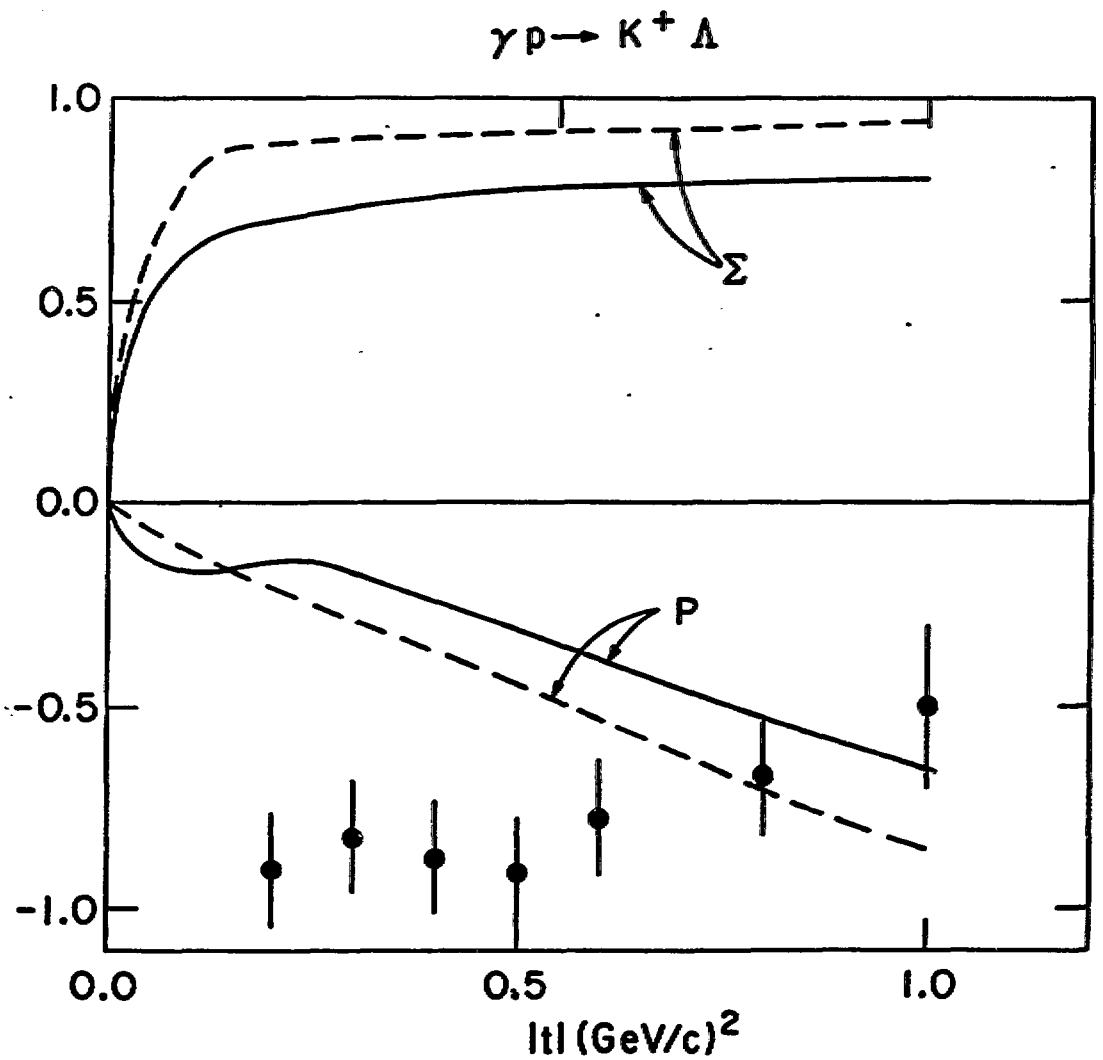

Neg. # 3-850-73

FIGURE 16